Lithos 318–319 (2018) 60–77

Contents lists available at ScienceDirect

Lithos

journal homepage: www.elsevier.com/locate/lithos

Interaction between mingling mafic and felsic magmas: Its roles in differentiation of a quartz monzonite and MMEs from eastern South China

Kong-Yang Zhu *, Zhong-Yue Shen, Ming-Yue Li, Yi-Hao Yu

School of Earth Sciences, Zhejiang University, 38 Zheda Road, Hangzhou, Zhejiang 310027, China

ARTICLE INFO

Article history:
Received 3 June 2018
Accepted 31 July 2018
Available online 3 August 2018

Keywords:
Mafic microgranular enclave
Magma mingling
Chemical diffusion
Magma differentiation
I-type granitoid

ABSTRACT

Compositional profiles and mapping of selected mafic microgranular enclaves (MMEs) in Muchen quartz monzonite in eastern South China give constraints on the interaction between mingling mafic and felsic magmas. The intrusion is a typical I-type MME-bearing magnetite-series granitoid in western Pacific. The MMEs and host quartz monzonite are not deformed and have similar magnetic fabrics, which does not support the MMEs are restites or earlier solidified mafic rocks but implies mafic magma globules flowed with felsic magma. The two MMEs represent mafic magma interacting with felsic magma at early and late stage, respectively. The late-stage MME has a Hbl-Bt-Kfs-Pl-Mag assemblage. The early-stage MME has a Cpx-Bt-Kfs-Pl-Mag assemblage with a rim similar to the late-stage MME. Acicular apatite implies rapid cooling of the mafic magmas; however, the similar isotopic ratios and mafic silicate compositions of the MME and quartz monzonite indicate partial equilibrium during magma interactions. Al-in-hornblende estimates the pluton emplacement at ~3.1–3.6 km and therefore the magma mingling-mixing still worked at shallow levels. Most trace element Harker diagrams do not produce linear variation trends and magma mixing cannot solo explain such a pattern. Enrichments of Na_2O, REE, Y, Nb, Ta, Ga, Fe^{3+} and depletions of K_2O, Rb, Ba, Sr in the MMEs through diffusion caused noticeable chemical differentiation of both mafic and felsic magmas. Therefore, mass transfer during magma mingling is an important mechanism influencing petrography and chemical compositions of I-type granitoids. Such processes may also extensively occur in the deep hot zones of the continental arc environments.

1. Introduction

Mafic microgranular enclave (MME) is commonly observed within granite and volcanic counterpart (Kumar and Rino, 2006). They are amongst large-scale heterogeneities in the granitic rocks (Barbarin and Didier, 1992). The genesis of MMEs is still considered as a controversial issue (Clemens et al., 2017), which may be also related to the genesis of appinites and lamprophyres (Ayrton, 1991). As argued by Baker (1990), "any magma containing enclaves is unlikely to retain its uncontaminated composition". However, some studies argue that although the enclaves necessarily reflect heat and material input from the mantle, they are not responsible for the main compositional variations in the granitoids (Clemens et al., 2016a, 2016b). Some quench textures (e.g., acicular apatite, fine-grained texture and chilling margins) appear to imply minor interactions between the MME and the host granite. Such a situation is referred to "magma mingling" (mechanical mixing) in some literatures (Don et al., 1997; Jerram and Petford, 2011). Nevertheless, the generally same mineral assemblages, similar mineral compositions and overlapped isotopic compositions between the MMEs and the host granitoids suggest equilibrium has been built during magma interactions (Didier and Barbarin, 1991).

Although it is suggested that detailed geochemical studies of core-to-host profiles, in large enclaves, are necessary to assess the importance of these equilibrium processes (Pin, 1991), few studies have been conducted in this way (Cramer and Kwak, 1988; Farner et al., 2014) and most were done on the bulk MME samples. As a result, the influences of such equilibria on the geochemical variations of the MMEs and host granites are not well understood. It is still less certain that whether the diffusion or other processes during magma mingling will significantly change the major and trace elemental compositions at the intrusion scale. In this study, we conducted in situ sampling on Early Cretaceous Muchen intrusion in eastern South China, which mainly comprises quartz monzonite hosting many MME swarms and represents a typical I-type granitoid with large geochemical variations in western Pacific margin. Zircon U—Pb dating and Hf isotopes as well as bulk Sr-Nd-Hf isotopes have been conducted for the intrusion by previous studies. New magnetic fabrics, bulk and mineral geochemical data are used to constrain the impact of shallow-level and potential deep-level magma mingling on the differentiations of I-type granitoids.

* Corresponding author.
E-mail address: zhukongyang@zju.edu.cn (K.-Y. Zhu).

https://doi.org/10.1016/j.lithos.2018.07.033
0024-4937/

These results improve the understanding of the geochemical evolutions of the intrusion relative to previous studies, suggesting the necessity of conducting in situ sampling during MME studies.

2. Geology and previous studies on Muchen quartz monzonite

The Muchen quartz monzonite (MQM) covers an area of ~58 km^2 in Zhejiang Province of eastern South China (Fig. 1A), representing one of late Early Cretaceous I-type granitoids in the region (Hsieh et al., 2009; Liu et al., 2013b; Wong et al., 2011; Zhu et al., 2014, 2017b). It is also a magnetite-series granitoid (Ishihara et al., 2000) with magnetite content obviously higher than other Mesozoic granitoids. Generation of these I-type rocks is commonly related to shallow-angle or flat-slab subduction of the paleo-Pacific Plate (Li and Li, 2007; Zhou and Li, 2000) and it is a result of continental lithospheric extension during roll-back of the oceanic plate. The MQM and related plutons also marked the end of fierce Mesozoic granitic magmatism in the region (Zhu et al., 2014). The Cathaysia Block, in which the MQM located, has the Paleoproterozoic basement known as Badu Complex (Yu et al., 2012). It amalgamated with the Yangtze Block in the northwest of South China during Neoproterozoic Sibao Orogen (Li et al., 2009). The MQM is a shallow-level (2.5–3.5 km) NNW-trending pluton that intruded the Badu Complex and early Early Cretaceous volcanics (Zhu et al., 2017b). The MQM has a massive structure and fine- to medium-grained

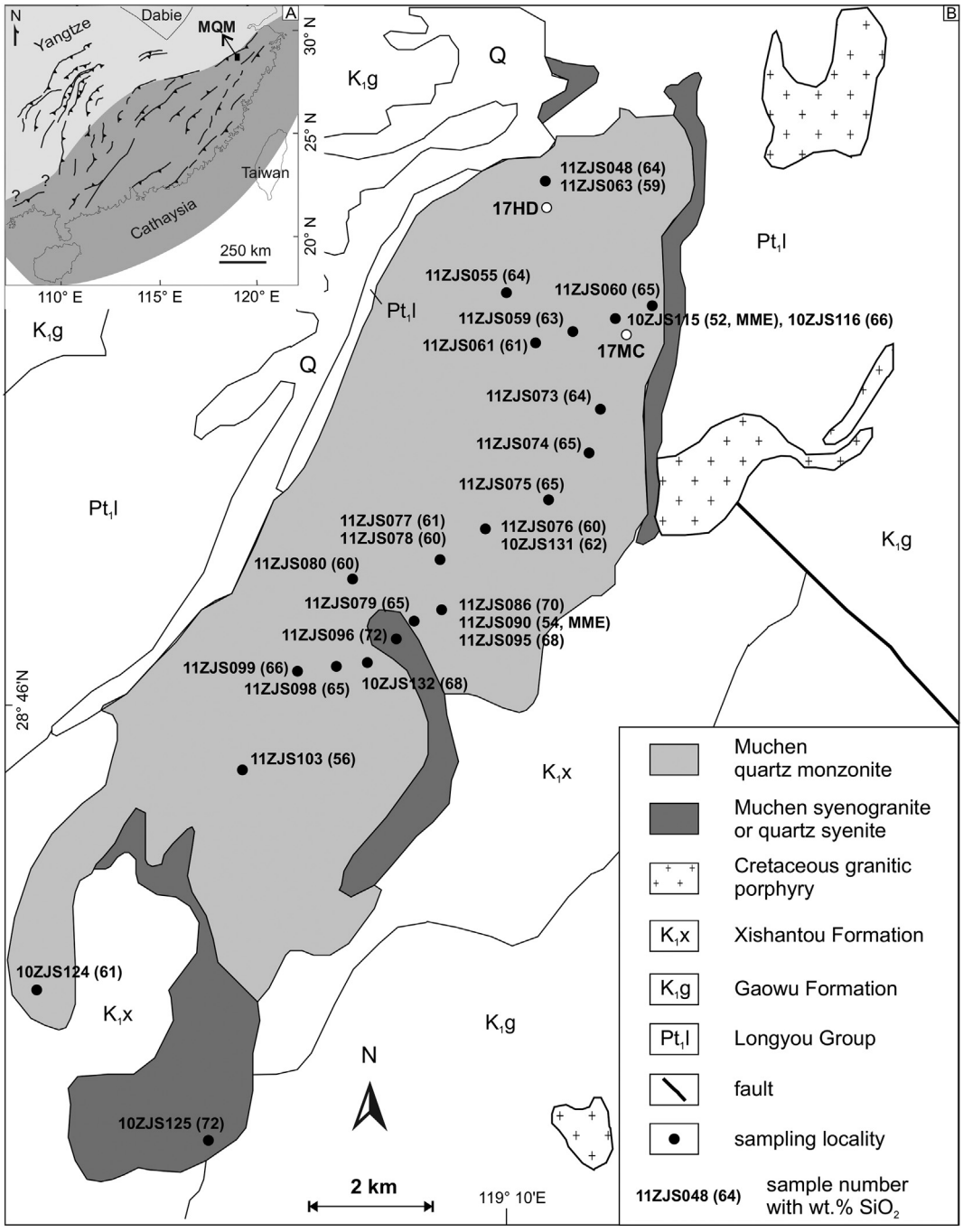

Fig. 1. A Tectonic map of South China, showing major Mesozoic thrust faults. The two components of the South China Block are Yangtze Block in the northwest and Cathaysia Block in the southeast (Li et al., 2010). The Muchen intrusion is located to the southeast of the boundary. B Geological map of the Muchen intrusion showing the major quartz monzonite unit intruded by the minor quartz syenite unit. However, the zircon U—Pb ages are indistinguishable for the two units. Sampling localities, with sample number and SiO_2 content (wt%), are also shown. 17MC and 17HD (open circles) are two MME-host pairs in this study; the others (solid circles) are published data (Zhu et al., 2014, 2017b).

texture, with the margin having finer grain sizes. The MQM mainly comprises quartz monzonite and was intruded by contemporaneous quartz syenite or syenogranite. As reported by ZGS (1966), the main minerals include K-feldspar (33–38%), plagioclase (40–46%), quartz (10–12%), biotite (1–3%), hornblende (7–8%) and magnetite (1–2%), with trace titanite, zircon, apatite, ilmenite and pyrite. The mineral assemblage is also common for other I-type granitoids in the region with similar ages, such as Matou, Liangnong and Xiaojiang plutons (Gao et al., 2014; Hsieh et al., 2009; Zhu et al., 2014).

The results of zircon U—Pb dating, conducted by Liu et al. (2013a) and Zhu et al. (2014), are the same for the MMEs and host granitoids, at around ~112 Ma. The inherited zircon is not found in the analyses. The bulk Sr-Nd-Pb isotopes and zircon Hf isotopes are also the same within the analytical errors. However, their isotopic compositions are different from those of the coeval basalts sourced from enriched mantle and earlier Late Triassic granitic rocks sourced from the crust (Zhu et al., 2017b). It supports that the isotopic features of the MQM were formed by magma mixing and isotopic equilibrium.

The MMEs are common in the MQM and appear to concentrate at the margin of the pluton (Zhu et al., 2017a). The size of most MMEs ranges from 1 cm to 20 cm. They are mostly rounded or ellipsoidal, occasionally elongated or sub-angular (Fig. 2). They occur as a single MME or a swarm in the outcrop. Most MMEs show sharp contacts with their host granitoids but diffuse contacts can be also found. The margins of MMEs are slightly finer-grained than the interiors and such chilling margins are not continuous, which can only be recognized under microscope. The previous studies (Zhu et al., 2014, 2017a) reported that the MMEs have a fine-grained texture, comprising ~69% plagioclase, ~17% hornblende, ~12% biotite, ~1% K-feldspar and quartz, ~1% magnetite, minor zircon and apatite. Some MMEs also contain clinopyroxene. Plagioclase zoning are common features in the MMEs, with calcic cores and sodic rims. The apatite grains are acicular or long prismatic, implying their rapid crystallization in the basic magma. Some MMEs contains K-feldspar phenocrysts with similar sizes to those in the host granite, most likely representing magma mingling. Blade biotite is typical in the MMEs, which is an unusual morphology

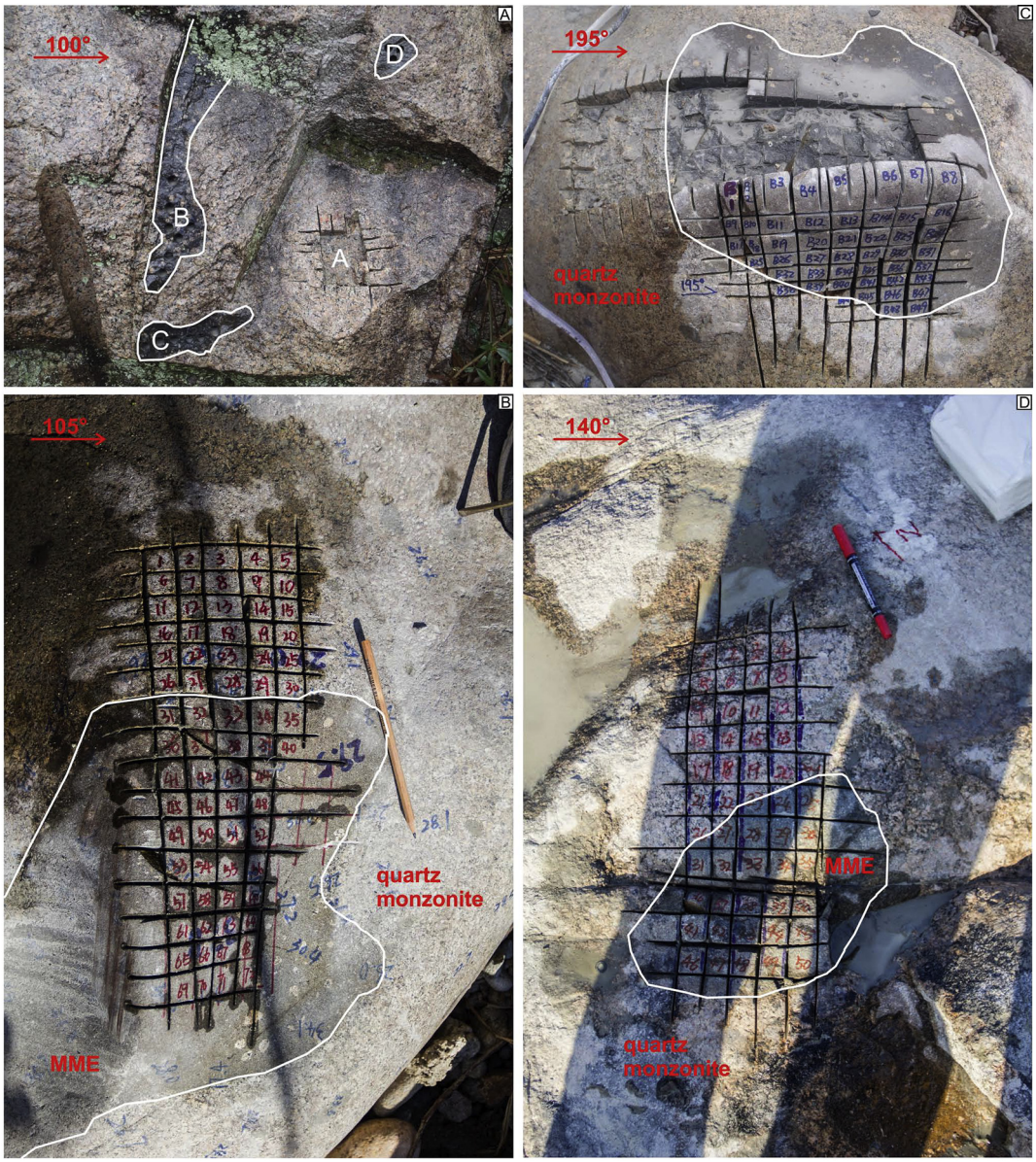

Fig. 2. A MME swarm at the sampling locality 10ZJS115 (see Fig. 1). The MMEs with different orientations have weak but common magnetic fabrics; the host quart monzonite at this locality show a random magnetic fabric. B the MME at the sampling locality 17MC, show the in situ sampling numbers. Some K-feldspar xenocrysts from the quartz monzonite are visible. C the same MME at the sampling locality 17MC, showing the sampling maps and sample numbers. D the MME at the sampling locality 17HD, with sample numbers.

of biotite that is prone to form during magma mixing (Hibbard, 1991). For many MME-granite pair, the magnetic fabrics are similar (Zhu et al., 2017a). The absence of straining of the minerals and strong variations of fabrics at different localities imply such similarities are caused by flow of mingled mafic and felsic magmas (Jerram and Petford, 2011).

On the TAS plot (Cox et al., 1979), most samples from the MQM are plotted in the alkaline field; on the SiO_2-K_2O plot (Peccerillo and Taylor, 1976), they belong to shoshonite series. They are mostly metaluminous or weakly peraluminous (A/CNK < 1.1), implying an igneous source. Most samples plot in the field of ferroan granitoid or straddle the boundary with magnesian granitoids (Frost and Frost, 2011), which are consistent with the proposed anorogenic setting. However, most samples have low Ga/Al ratios and are not typical A-type granitoids, except for the most felsic ones from the syenogranite/quartz syenite unit. Isotopic compositions are similar for the quartz monzonite, syenogranite/quartz syenite and MME (Zhu et al., 2014; Zhu et al., 2017b), with whole-rock I_{Sr} ranging from 0.7053 to 0.7070, εNd(t) from −3.8 to −1.3, $(^{206}Pb/^{204}Pb)_t$ from 17.98 to 18.07, $(^{207}Pb/^{204}Pb)_t$ from 15.58 to 15.62 and $(^{208}Pb/^{204}Pb)_t$ from 38.47 to 38.70. Zircon εHf (t) values are clustered around zero, ranging from −4 to 4.

Geological and geochemical study on the MQM started >50 years ages ago (ZGS, 1966). Magma mixing, as supported by existence of MMEs, is often invoked as the major mechanism for magma differentiation (Liu et al., 2011; Liu et al., 2012, 2013a; Lu, 2007). However, like other cases (Clemens et al., 2016b; Clemens et al., 2017), curvilinear trends for some major and trace elements are difficult to understand unless several magma sources or other processes were involved. Previous sampling of MMEs have not covered any profile from the core of MME to the host quartz monzonite. A lack of detailed core-host analyses, as Pin (1991) suggested, hampers the understanding of the mixing mechanism.

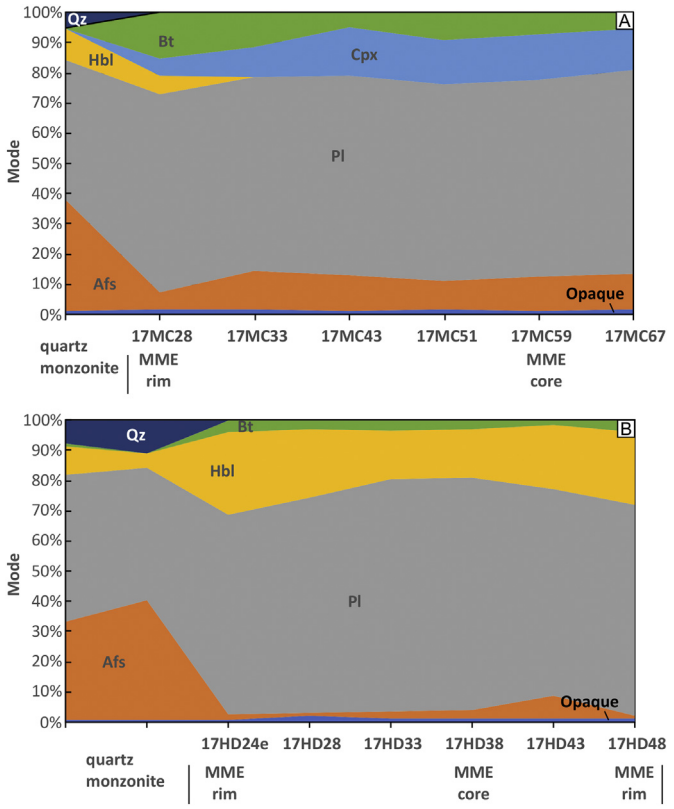

Fig. 4. Modes of the two MME-quartz monzonite profiles: A 17MC, B 17HD. Biotite occurs in the quartz monzonite of both profiles, but in low proportions.

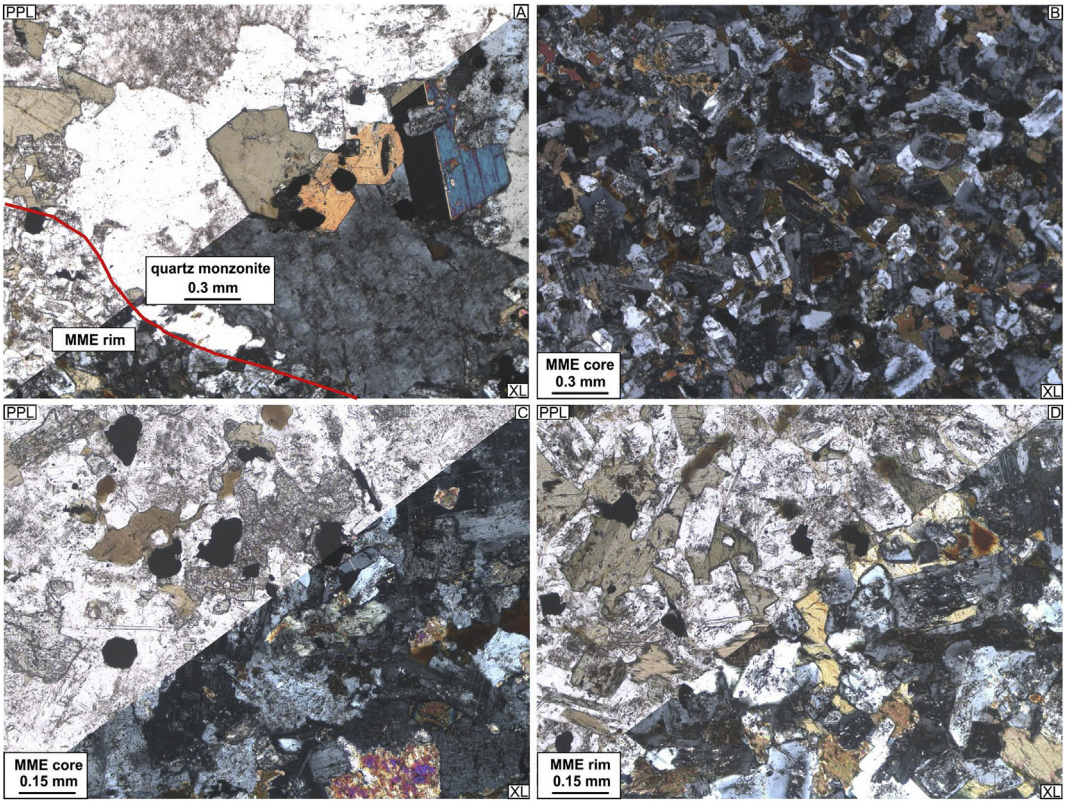

Fig. 3. Photomicrographs of the MME-host quartz monzonite pair (17MC). A Subhedral hornblende in quartz monzonite in a sharp contact with the MME. B the core of the MME, showing the intergranular to subophitic texture and zoning texture of plagioclase. C the core of the MME, showing colorless clinopyroxene, brown biotite, magnetite and acicular apatite. D the rim of the MME, showing green-brown hornblende, brown biotite, magnetite and acicular apatite.

3. Sampling, analytical methods and modes

Samples are collected in situ for petrography, anisotropy of magnetic susceptibility (AMS) and geochemical analyses. ~2 cm cubes were sampled using a portable tile cutter and 0.9-cm-diameter cylinders were sampled by a portable drill for small-sized MMEs for AMS study. Detailed maps of sampling are shown in Fig. 1B. The instruments and methods for whole-rock major and trace elemental analyses and AMS studies are the same as described in Zhu et al. (2017b) and Zhu et al. (2017a), respectively. Geochemical analyses were conducted on two MME-host granitoid profiles (17MC and 17HD) and the MME of 17MC was also mapped for trace element compositions (Fig. 2). Marginal granitic parts of the MMEs were removed before powdering to minimize contamination, using a grinding machine (Zhu et al., 2017a). Electron probe analyses for mafic silicates and feldspars from 17MC were conducted on a JEOL 8100 EPMA (Second Institute of Oceanography, China) and a SHIMADZU 1720 EPMA (Zhejiang University, China), respectively. Both operated at a probe current of 2×10^{-8} A and an accelerating voltage of 15 kV. An electron beam diameter of 5 μm was used for amphibole, alkali feldspar, plagioclase and clinopyroxene; 15 μm was used for biotite.

The modal analyses were conducted on a series of thin sections of the aforementioned MME-granitoid pairs, using the pixel statistic function of Adobe Photoshop on microphotographs and backscatter electron images. In general, the mafic silicates, mainly hornblende, in the host granites are euhedral or subhedral (Fig. 3). The alkali feldspar (Afs) in

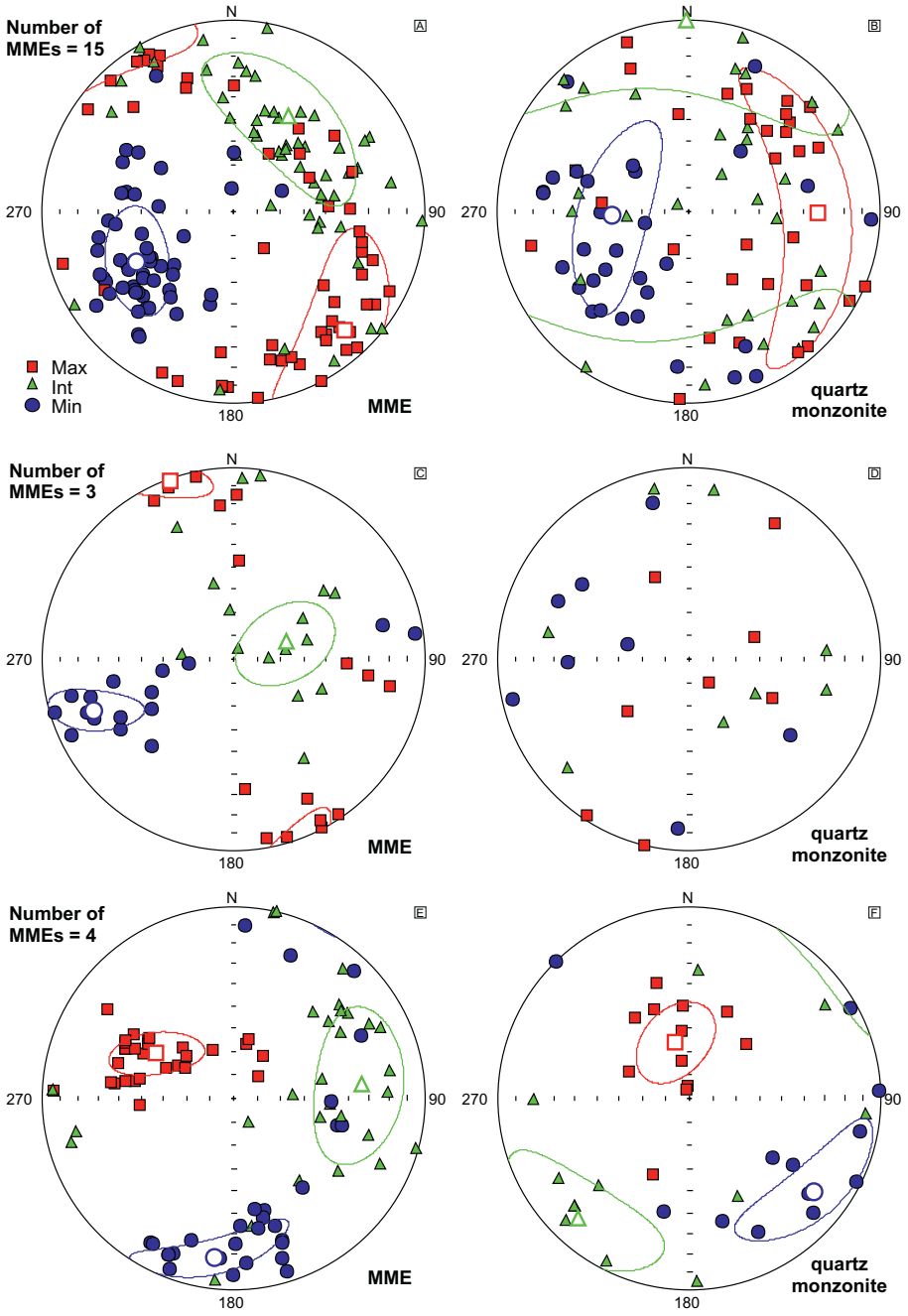

Fig. 5. AMS results with the mean tensors and 95% confidence ellipses (Schmidt plots with lower hemisphere and equal area projection, in present geographic orientation) for three MME swarms and host quartz monzonite at sampling locality 17MC (A, B), 10ZJS115 (C, D) and 17HD (E, F). In each pair, the MME swarm has the same magnetic fabrics, implying they used to be coherent magma flow or linked by magmatic flow processes; however, the host quartz monzonite may have similar magnetic lineation/foliation orientations to the hosting MME swarm or show random magnetic fabrics.

Table 1
Composition of alkali feldspar and plagioclase in MME-quartz monzonite pair (17MC).

Mineral	Analysis	SiO_2	Al_2O_3	CaO	Na_2O	K_2O	Total	Or	Ab	An
17MC28, quartz monzonite at the boundary										
Afs-p[a]	Ksp-11	65.49	19.27	0.67	4.60	9.28	99.32	55.1	41.5	3.4
Afs-g[b]	ksp-15	64.54	17.84	0.01	0.49	16.26	99.14	95.6	4.4	0.0
Pl-core	pl-11c	61.50	23.85	6.07	7.96	0.38	99.75	2.1	68.8	29.0
Pl-rim	pl-11r	62.68	22.92	4.87	8.44	0.41	99.32	2.4	74.0	23.6
17MC28, MME at the boundary										
Afs	Ksp-4	64.86	18.39	0.00	0.70	16.10	100.05	93.8	6.2	0.0
Pl-core	pl-2c	56.91	26.70	8.99	6.20	0.17	98.96	1.0	55.0	44.0
Pl-rim	pl-2r	63.90	22.59	4.05	9.20	0.37	100.10	2.1	78.8	19.1
17MC33, MME at the rim										
Afs	KSP-6	65.44	18.28	0.08	0.58	16.33	100.70	94.5	5.1	0.4
Pl-core	PL-2C	53.53	29.38	11.93	4.52	0.11	99.60	0.6	40.4	58.9
Pl-rim	PL-2R	62.11	23.95	5.37	8.25	0.19	99.92	1.1	72.7	26.2
17MC43, MME at the core										
Afs	KSP-2	64.86	18.04	0.00	0.68	15.77	99.40	93.8	6.2	0.0
Pl-core	PL-4C	50.90	30.53	14.05	3.66	0.09	99.26	0.5	31.8	67.6
Pl-rim	PL-4R	60.76	24.29	6.36	7.71	0.24	99.41	1.4	67.8	30.9
17MC51, MME at the core										
Afs	KSP-7	64.73	18.10	0.04	0.69	15.86	99.58	93.6	6.2	0.2
Pl-core	PL-6C	52.51	29.18	13.26	4.11	0.11	99.52	0.6	35.7	63.7
Pl-rim	PL-6R	61.61	23.75	6.20	7.57	0.25	99.37	1.5	67.8	30.7
17MC59, MME at the core										
Afs	KSP-3	65.58	16.99	0.04	0.81	15.82	99.62	92.6	7.2	0.2
Pl-core	PL-3C	51.85	30.19	13.20	3.93	0.12	99.43	0.7	34.8	64.5
Pl-rim	PL-3R	61.60	23.77	5.89	8.05	0.28	99.64	1.6	70.0	28.4

[a] Phenocryst
[b] Groundmass

the host quartz monzonite has two generations: earlier euhedral phenocrysts and later fine-grained anhedral ones. The plagioclase (Pl) generally forms euhedral grains. The mafic silicates in the MME, including biotite (Bt), hornblende (Hbl) and clinopyroxene (Cpx), form intergranular to subophitic texture with euhedral zoned plagioclase. Quartz (Qz) is anhedral in the host quartz monzonite but not found in the MMEs. The host quartz monzonites of 17MC and 17HD show little differences. However, the MME of 17MC has a core containing Bt-Cpx and a rim (0.5–1 mm, not uniform thickness) with slightly finer-grained texture containing Bt-Hbl. In contrast, the MME of 17HD contains Bt and Hbl but no Cpx. It appears that different degrees of magma interaction caused such results and the MME of 17HD is a more evolved one. There exist K-feldspar phenocrysts in the MMEs; however, their distribution is not uniform within and between the MMEs. They are likely from the host granite through mingling processes. The acicular apatite grains in the MMEs, like many other cases, reflect their rapid crystallization (Vernon, 1984). The opaque minerals are predominately magnetite, but ilmenite and pyrite are occasionally observed. The modal results, from the host quartz monzonites to the core of MMEs, are shown in Fig. 4. In general, the MME contains high modal Pl and mafic silicate; the host quartz monzonite contains high modal alkali feldspar and quartz.

4. Analytical results

4.1. Anisotropy of magnetic susceptibility (AMS)

As recognized by Zhu et al. (2014), the magnetic susceptibilities of the MQM, as well as other 115–100 Ma granitoids and their MMEs, are significantly higher than older Mesozoic granitoids. These intrusions are also characterized by obvious aeromagnetic anomalies due to their high magnetite contents. The κ-T and X-ray computed tomography analyses confirmed the magnetic susceptibility and anisotropy of the MQM are controlled by the contents and sharp-anisotropy of multi-domain magnetite, respectively (Zhu et al., 2017a). The results from the new samples are generally consistent with the previous study (Zhu et al., 2017a). For some MMEs, magnetic susceptibility measurements on their margins tend to yield the larger values. The magnetic fabrics are very weak and change significantly from outcrop to outcrop (Fig. 5). This supports these are magmatic fabrics in these non-deformed rocks. Such fabrics are different from the fabrics caused by dynamic metamorphism. The MME swarm at an outcrop commonly has similar magnetic fabrics (Fig. 5A, C, E). In some cases, they are also similar to those of the host granitoids (Fig. 5B, F). At the locality of 17MC, the MMEs and their host quartz monzonite have the same foliation

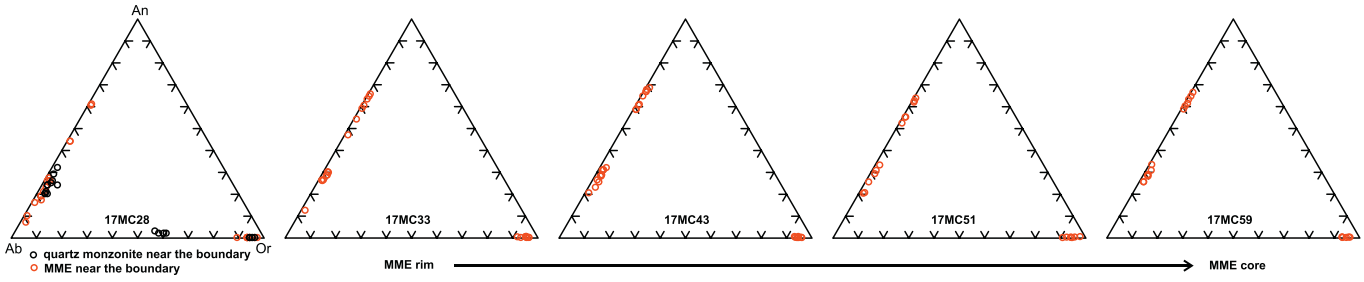

Fig. 6. Compositional variations of plagioclase and alkali feldspar from the quartz monzonite-MME pair (17MC). The early euhedral alkali feldspar grains are more Ab-rich than the late ones. The plagioclase grains (both rim and core) at the MME rim are more sodic than those in the MME core.

Table 2
Composition of biotite, hornlende and clinopyroxene in MME-quartz monzonite pair (17MC).

Sample	MC28				MC28				MC33					MC59			
Position	granite at the boundary				MME at the boundary				MME rim					MME core			
Mineral	Bt	Bt	Hbl	Hbl	Bt	Bt	Hbl	Hbl	Bt	Bt	Hbl	Cpx	Cpx	Bt	Bt	Cpx	Cpx
Analysis	1	9	11	14	35	36	17	18	15	17	5	2	14	10	16	2	3
SiO_2	36.02	36.18	46.53	46.16	36.89	37.02	46.44	46.35	36.17	37.38	46.98	50.63	51.18	36.80	36.37	52.41	52.66
TiO_2	4.43	4.68	1.40	1.33	4.44	4.42	1.26	1.50	4.92	4.61	1.10	0.54	0.42	4.71	4.89	0.25	0.12
Al_2O_3	12.89	13.28	5.79	6.15	12.82	12.36	5.77	6.40	12.91	12.85	5.71	2.51	2.09	12.86	13.07	1.38	0.72
FeO	21.21	22.62	17.56	17.14	21.32	21.49	17.41	17.27	22.30	19.70	18.46	11.00	10.40	21.76	19.76	8.41	12.43
MnO	0.35	0.51	0.87	0.92	0.45	0.44	1.01	0.86	0.37	0.33	1.09	0.94	0.82	0.31	0.50	0.46	1.25
MgO	10.72	9.44	12.41	12.30	10.57	10.89	12.20	12.15	9.61	12.05	11.79	12.25	12.54	10.33	11.88	13.87	12.74
CaO	0.03	0.02	10.34	10.64	0.04	0.04	10.50	10.80	0.39	0.08	10.59	21.64	21.59	0.03	0.01	22.62	20.41
Na_2O	0.27	0.16	1.81	2.01	0.18	0.22	1.84	1.86	0.14	0.15	1.73	0.50	0.46	0.16	0.24	0.39	0.28
K_2O	9.42	9.40	0.75	0.81	9.36	9.47	0.69	0.81	9.39	9.30	0.70	–	0.00	9.41	9.36	0.00	0.02
F	1.08	0.89	1.07	1.03	0.96	1.02	0.90	0.93	0.75	1.07	0.90	–	–	0.81	1.13	–	–
Cl	0.51	0.47	0.23	0.25	0.49	0.36	0.20	0.23	0.53	0.49	0.37	–	–	0.44	0.46	–	–
Cr_2O_3	0.05	0.03	0.02	0.03	–	–	0.03	0.00	0.04	–	0.06	–	0.03	0.03	0.00	–	0.01
NiO	–		0.01	0.01	0.01	–	0.06	0.03	0.06	–	0.07	0.05	–	–	0.01	0.00	–
O=F,Cl	0.57	0.48	0.50	0.49	0.51	0.51	0.42	0.44	0.43	0.56	0.50	–	–	0.44	0.58	–	–
Total	96.42	97.20	98.29	98.28	97.02	97.22	97.89	98.74	97.13	97.44	99.04	100.06	99.55	97.19	97.10	99.79	100.64

orientations (Zhu et al., 2017a). At the locality of 17HD, the MMEs and their host rocks have similar lineation orientations. At the locality of the MME sample 10ZJS115 (Zhu et al., 2014), the MME swarms have common foliation orientations whereas the host rock shows random AMS (Fig. 5C, D). The magnetic fabrics are in some cases not consistent with the shape anisotropy of the MME (cf. Fig. 2A). It probably reflects the MMEs cannot freely adjust the orientation in highly viscous granitic magmas or the shapes of MMEs have been further modified (partly digested) even after the cease of magma flow. The consistent magmatic fabrics of MME swarms do not support that they are solid mafic rocks (restite, older mafic rock, etc.) transported to shallow levels by granitic magmas (Chappell et al., 1987).

4.2. Mineral chemistry

4.2.1. Plagioclase and alkali feldspar

The representative results and end-members (Ab-An-Or) compositions of feldspars from the MME-quartz monzonite pair at sampling locality 17MC are given in Table 1 and Fig. 6. The plagioclase grains in the quartz monzonite have compositions of $An_{14–32}$ and the cores are slightly more calcic. The plagioclase grains in the center of the MME are more calcic than those at the rim. The zoned grains at the rim of the MME have cores of $An_{44–61}$ and rims of $An_{10–26}$; whereas most of the zoned grains in the center of the MME have cores of $An_{\sim 60–70}$ and rims of $An_{\sim 25–35}$.

Alkali feldspar in both MME and quartz monzonite is orthoclase. In the quartz monzonite, the alkali feldspar has two generations. The euhedral phenocrysts have compositions of $Or_{55–60}Ab_{38–42}An_{2–3}$ and the interstitial ones have a composition of $Or_{93–96}Ab_{4–6}$. In the MME, the alkali feldspar is interstitial and has a composition of $Or_{89–97}Ab_{11–7}$.

4.2.2. Biotite, hornblende and clinopyroxene

Biotite is a prevalent ferromagnesian mineral in the MQM, both in MMEs and host rocks, occurring as subhedral grains. The representative biotite compositions from the MME-quartz monzonite pair at sampling locality 17MC are shown in Table 2 and Fig. 7A, together with hornblende and clinopyroxene. Structural formula is calculated based on 24 (O,OH,F,Cl). The biotite crystals from the core of the MME to the host quartz monzonite have similar compositions. Such similarities were not recognized by Vernon (1984) but have been found in many other studies (Didier and Barbarin, 1991; Kumar and Rino, 2006; Tepper and Kuehner, 2004). In terms of Fe/(Fe + Mg)–Si binary components (Deer et al., 1962), they are plotted in the field of biotite, with most analyses having Fe/(Fe + Mg) = 0.48–0.59 and Si (a.p.f.u.) = 5.5–5.8. Negative linear correlation between Mg and Fe in these analyses suggests that Mg—Fe substitution prevailed in felsic-mafic magma

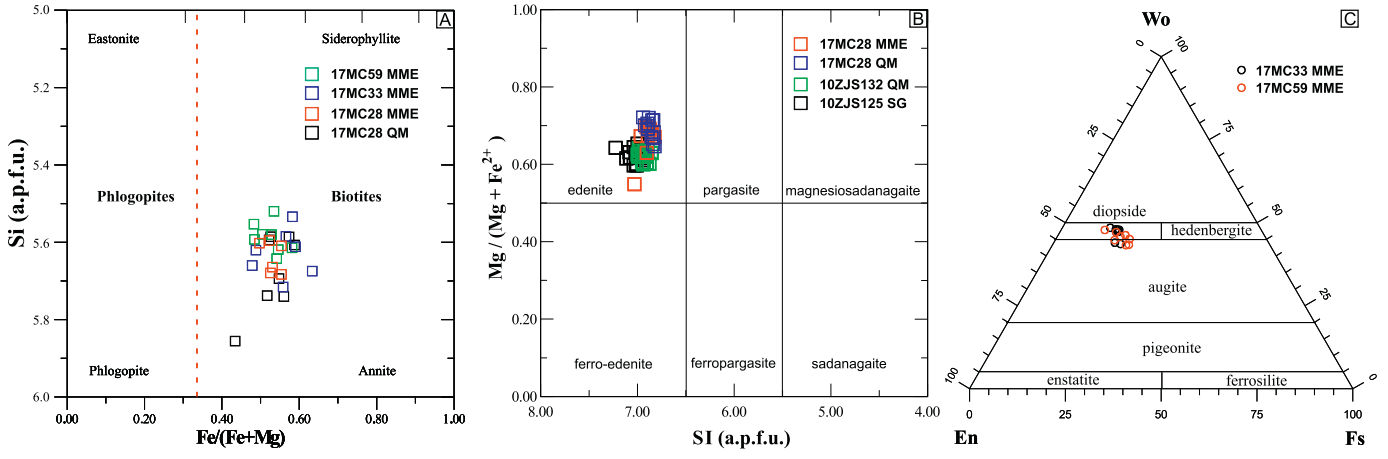

Fig. 7. Compositions of biotite (A), hornblende (B) and clinopyroxene (C) from the quartz monzonite-MME pair (17MC) from this study and a previous study (Zhu et al., 2017b). The biotite analytical results are similar for the MME and host quartz monzonite. The analytical results of hornblende from the MME-quartz monzonite pair (17MC), MME-absent quartz monzonite (10ZJS132) and syenogranite (10ZJS125) are also similar. The clinopyroxene analyses from the core of the MME are plotted in the field of diopside or augite.

mixing system (Kumar and Rino, 2006). Based on the tectonic discrimination diagram of Abdel-Rahman (1994), they straddle the boundary between anorogenic alkaline suites and calc-alkaline orogenic suites in FeO_t–MgO–Al_2O_3 space.

In the analyzed MME-quart monzonite pair, the euhedral to subhedral hornblende is the dominating mafic silicate in the host rock; however, in the MME, much finer-grained subhedral ones are only distributed at the rim. Structural formula is calculated based on 24 (O,OH,F,Cl). The compositions of the hornblende from the MME and host rocks, like the biotite, are overlapped. On the basis of the standard International Mineralogical Association (IMA-04) classification procedure, they are plotted in the field of edenite (Fig. 7B). The thermobarometric formulations of Ridolfi et al. (2009) yield temperatures of 784–858 °C, pressures of 81–95 MPa and oxygen fugacities between QFM + 1.7 and QFM + 2.2. A shallow emplacement level (~3.1–3.6 km) is therefore implied.

Clinopyroxene, occurring in the MME 17MC except for its rim, was analyzed with 15 spots. The results are plotted in the field of either diopside or augite (Fig. 7C). The clinopyroxene grains show no significant differences for different parts of the MME.

It is often stated that the MMEs and their host granitoids have the same types of mafic silicates and the compositions of these minerals are also similar (Didier and Barbarin, 1991). Recent studies stressed it is the intensive parameters (P, T, water and oxygen fugacity) that largely control the compositions of amphibole and biotite in subduction-related magmatic rocks (Anderson et al., 2008; Ridolfi et al., 2009; Wones, 1981). Therefore, the same compositions of biotite and hornblende in the MME-quartz monzonite pair indicate equilibria of these intensive parameters. Considering other samples from the Muchen intrusion also have similar hornblende compositions (Zhu et al., 2017b), such equilibria are likely intrusion-scale as the case for the isotopic equilibria.

4.3. Whole rock chemistry

The whole-rock major and trace element data of the two MME-host profiles (17MC and 17HD) are shown in Tables 3 and 4, respectively. The mapping results of the MME 17MC are shown in Appendix A. In the compositional profiles from the host quartz monzonite to the MME core (Fig. 8), SiO_2 and K_2O dive and TiO_2, Al_2O_3, FeO_t, MgO, CaO, P_2O_5 jump across the boundary. The MME margins have the highest Na_2O and Fe_2O_3t as well as the lowest K_2O contents in the profiles. The Fe_2O_3t maximum is caused by the highest Fe_2O_3 at the margin, as shown by the 17MC profile. This trend is masked by the pyritization alteration at the MME margin for the 17HD profile. In the two MME-quartz monzonite profiles, the MME margins have lower Ba, Cs, Rb, Zr,

Table 3
Major (wt%) and trace (ppm) elements of the early-stage MME and host quartz monzonite (17MC) in the Muchen intrusion.

Sample	6	11	16 + 17	21	26	31	36	41	45	49	53	57	61	65	69
Locality	Quartz monzonite					MME									
SiO_2	63.18	62.97	62.93	63.22	63.68	53.51	53.77	53.84	53.19	53.17	53.57	53.43	53.26	53.33	53.07
Al_2O_3	15.87	16.06	16.44	15.90	15.92	17.43	17.60	17.84	17.56	17.48	17.65	17.61	17.72	17.61	17.65
TiO_2	0.43	0.42	0.45	0.43	0.42	0.93	0.93	0.91	0.91	0.95	0.93	0.95	0.92	0.94	0.95
Fe_2O_3	0.64	0.93	1.58	0.98	0.95	3.02	2.44	1.99	2.19	2.15	2.38	2.02	2.05	2.07	2.25
FeO	4.60	4.62	3.54	4.29	4.09	6.39	6.53	6.00	6.12	6.35	5.75	6.13	6.18	6.18	5.95
MgO	1.06	1.11	1.15	1.06	1.14	2.43	2.51	2.55	2.54	2.67	2.60	2.70	2.62	2.64	2.68
MnO	0.16	0.16	0.15	0.15	0.16	0.24	0.24	0.25	0.31	0.30	0.26	0.31	0.29	0.31	0.29
CaO	2.34	2.77	2.88	2.59	2.70	5.03	5.46	5.68	5.62	5.86	5.76	5.95	5.81	5.86	5.94
K_2O	5.49	4.81	4.92	5.48	5.43	3.25	3.72	3.89	3.87	3.81	3.86	3.97	3.88	3.83	3.80
Na_2O	4.11	4.39	4.43	4.08	4.16	4.85	4.55	4.51	4.37	4.36	4.34	4.27	4.32	4.29	4.32
P_2O_5	0.23	0.25	0.25	0.23	0.24	0.64	0.63	0.62	0.62	0.63	0.64	0.65	0.63	0.64	0.64
SrO	0.05	0.05	0.05	0.05	0.05	0.06	0.07	0.08	0.08	0.09	0.08	0.09	0.09	0.09	0.09
BaO	0.07	0.06	0.06	0.06	0.08	0.04	0.07	0.07	0.08	0.08	0.08	0.09	0.08	0.08	0.08
LOI	0.78	0.50	0.58	0.44	0.46	1.25	0.75	0.83	0.89	0.84	1.10	0.99	0.96	1.05	0.90
Total	99.01	99.10	99.41	98.96	99.48	99.06	99.28	99.06	98.35	98.74	99.00	99.16	98.81	98.92	98.61
Ba	595	516	525	578	665	381	556	621	659	669	679	686	703	671	671
Ce	69.7	76.0	80.0	73.1	79.0	115.4	88.7	81.2	80.0	74.5	73.2	77.3	81.7	76.1	81.1
Cs	2.81	2.51	2.59	2.62	2.57	6.35	9.51	8.14	7.69	8.25	7.44	7.94	7.69	7.26	7.94
Dy	5.16	5.80	5.82	5.61	6.17	7.13	5.03	5.19	5.06	5.23	5.08	4.99	5.08	4.84	5.20
Er	3.12	3.55	3.63	3.48	3.66	4.09	2.66	2.81	2.76	2.64	2.70	2.71	2.76	2.70	2.86
Eu	1.15	1.17	1.17	1.17	1.34	1.39	1.56	1.78	1.85	1.93	2.02	1.96	2.04	1.94	1.88
Ga	17.8	17.8	18.1	16.8	16.9	20.6	18.3	17.0	17.2	17.2	17.1	16.9	16.9	17.2	17.6
Gd	6.10	6.50	6.60	6.42	6.86	9.31	6.83	6.96	6.46	6.91	6.99	6.89	7.14	6.82	6.86
Hf	6.7	7.4	7.5	7.3	7.4	4.3	3.5	4.2	5.8	6.2	6.4	6.1	6.3	6.4	6.3
Ho	1.00	1.13	1.14	1.13	1.19	1.45	0.96	0.98	0.96	1.00	0.95	0.96	0.96	0.92	0.96
La	34.0	37.6	39.2	35.1	37.1	62.5	52.0	47.5	44.6	42.2	40.4	43.5	46.6	42.2	45.1
Lu	0.54	0.57	0.61	0.56	0.60	0.63	0.39	0.42	0.40	0.39	0.36	0.38	0.39	0.37	0.41
Nb	23.2	23.3	24.9	22.0	22.1	24.9	17.1	14.2	13.0	12.2	11.4	11.3	11.4	11.3	12.1
Nd	32.1	35.6	38.2	33.8	37.5	54.8	39.9	38.2	35.6	35.6	35.4	35.9	37.3	34.5	35.6
Pr	8.34	9.13	9.78	8.88	9.50	14.16	10.31	9.70	9.01	8.84	8.75	8.79	9.35	8.51	9.04
Rb	250	205	213	224	219	261	302	285	282	287	278	288	289	285	295
Sm	6.44	6.91	7.28	6.79	7.46	10.38	7.37	7.25	6.83	7.10	7.30	7.03	7.26	6.91	6.98
Sn	4	5	3	2	3	6	6	3	4	3	3	3	3	3	3
Sr	437	461	486	453	514	574	638	704	760	814	828	825	821	811	817
Ta	1.5	1.6	1.6	1.4	1.3	1.2	0.8	0.7	0.6	0.6	0.6	0.6	0.6	0.6	0.6
Tb	0.88	0.95	1.02	0.94	1.05	1.33	0.90	0.92	0.91	0.93	0.96	0.92	0.95	0.93	0.90
Th	21.5	21.0	17.45	16.60	18.70	9.20	8.91	7.05	6.25	5.66	5.69	5.60	5.72	5.92	5.99
Tm	0.49	0.56	0.55	0.54	0.56	0.64	0.39	0.42	0.38	0.40	0.41	0.39	0.40	0.39	0.39
U	3.81	3.74	3.70	3.53	3.49	2.93	2.33	1.85	1.89	1.62	1.58	1.54	1.45	1.46	1.60
V	48	63	51	46	50	120	125	127	128	126	119	125	130	129	140
W	2	11	1	1	1	2	1	1	1	1	1	1	1	1	2
Y	28.7	31.4	33.3	30.2	34.4	42.6	27.9	27.6	27.8	28.3	27.8	27.5	27.1	27.4	28.4
Yb	3.47	3.65	3.84	3.68	3.89	4.08	2.56	2.62	2.51	2.61	2.41	2.44	2.46	2.43	2.53
Zr	259	264	301	264	290	171	116	174	284	293	301	281	288	297	297

Hf contents than the cores and in many cases their contents are the lowest in the profiles. The MME margins have higher REE, Ga (and Ga/Al), Nb, Ta contents than the cores and in many cases their contents are the highest in the profiles (Fig. 8). Sr and Eu tend to decrease continuously from the MME cores to the quartz monzonite. But in one of the profiles, Sr (but not Eu) shows a sudden drop, which is likely caused by late alteration. Comparing the two profiles, the MME 17HD is generally more evolved than the MME 17MC, since the trace elemental contents of 17HD appear to be further modified on the basis of 17MC. Mapping of the 17MC MME shows similar results with the one-dimensional compositional profiles (Fig. 9 and Appendix A). Nb, U, Th, REE (except for Eu), Y and Ga are higher at the margin; however, Ba, Sr, Eu, Rb and Zr are lower. LREE/HREE and MREE/HREE are both lower at the margin.

Considering the data of quartz monzonite at both outcrop-scale and intrusion-scale (Fig. 10), the samples close to the MMEs tend to have the lowest contents of Ga, La, Ce, Fe_2O_3 and the highest content of Rb, at the same SiO_2 contents. These granitic samples tend to develop lower La/Yb, La/Sm and Ga/Al ratios (Fig. 11). Nb and Th contents are also relatively low in the samples close to the MMEs.

The Al-factor versus Fe-factor diagrams (Cramer and Kwak, 1988) well demonstrate the mafic mineral assemblages in the MME-quartz monzonite pair (Fig. 12). For the quartz monzonite and the margin of the MME, the bulk compositions are plotted along the line linking hornblende and magnetite, consistent with rarity of biotite in these samples; For the interior of the MMEs, the bulk compositions are plotted between clinopyroxene, biotite and magnetite, and their inferred proportions are also consistent with petrography. In addition, as shown in Fig. 12B, the two samples at the MME margin have higher Fe-factors and are plotted closer to magnetite, which is consistent with higher magnetite susceptibility at the margin. A similar case can be found in Zhu et al. (2017b). Another point linking the mineral chemistry, whole-rock chemistry and magnetite susceptibility is that MME, intermediate and felsic samples all have high magnetite contents. Although the mode of the total ferromagnesian minerals decreases; the proportion of magnetite in these minerals will increase with higher Al-factor and Fe-factor in more evolved rocks (Fig. 12A).

5. Discussion

5.1. The role of magma mingling in evolution of I-type granitoids and their MMEs

Comparing to magma mixing, magma mingling is considered as a mechanical process whereby the felsic and mafic magmas retain their compositional integrity (Jerram and Petford, 2011). Magma mixing

Table 4
Major (wt%) and trace (ppm) elements of the late-stage MME and host quartz monzonite (17HD) in the Muchen intrusion.

Sample	7	11	15	19	23	25	30	34 + 35	40	45	50
Locality	Quartz monzonite					MME					
SiO_2	64.58	67.38	63.24	64.23	63.07	52.20	51.85	52.55	52.67	51.83	51.77
Al_2O_3	16.15	15.27	16.18	16.75	16.78	17.78	17.62	17.78	17.74	17.70	17.82
TiO_2	0.36	0.26	0.42	0.36	0.42	1.00	1.02	1.03	0.98	1.02	1.02
Fe_2O_3	1.32	0.95	1.57	1.06	1.29	2.94	3.32	4.32	3.80	3.81	3.66
FeO	2.98	2.46	3.37	2.85	3.08	6.90	6.88	5.79	5.70	6.06	6.27
MgO	0.95	0.61	1.11	0.87	1.05	3.08	3.17	3.06	2.95	3.11	3.19
MnO	0.17	0.14	0.20	0.17	0.17	0.37	0.42	0.36	0.32	0.32	0.34
CaO	2.00	1.49	2.65	2.22	2.47	4.65	4.86	4.58	4.36	4.72	4.61
K_2O	6.13	6.33	5.12	5.84	5.21	1.52	1.78	2.22	2.37	2.19	1.61
Na_2O	4.04	3.71	4.39	4.33	4.44	5.57	5.29	5.12	5.10	4.99	5.45
P_2O_5	0.19	0.12	0.24	0.18	0.24	0.75	0.77	0.76	0.73	0.76	0.77
SrO	0.06	0.05	0.06	0.06	0.06	0.09	0.09	0.09	0.09	0.09	0.09
BaO	0.09	0.07	0.07	0.08	0.08	0.04	0.05	0.06	0.05	0.06	0.04
LOI	0.71	0.56	0.55	0.57	0.78	1.83	1.81	1.98	1.96	2.17	2.15
Total	99.73	99.40	99.17	99.57	99.14	98.72	98.93	99.70	98.82	98.83	98.79
Ba	748	636	594	730	671	294	421	448	425	435	301
Ce	89.6	83.8	88.2	99.6	74.5	118.5	104.5	98.4	96.4	97.9	114.0
Cs	4.42	4.66	3.98	4.29	4.64	7.09	8.16	8.22	7.51	6.94	6.66
Dy	4.71	3.35	5.86	4.56	4.61	7.71	7.03	6.78	7.26	7.03	7.77
Er	2.88	2.05	3.47	2.66	2.74	4.60	4.06	3.90	4.25	4.25	4.51
Eu	1.24	1.00	1.33	1.31	1.35	1.43	1.47	1.54	1.57	1.62	1.54
Ga	17.5	16.8	17.3	17.1	17.7	22.8	21.2	20.1	19.7	21.0	22.0
Gd	5.77	3.94	7.23	5.72	5.64	10.15	9.58	8.90	9.28	9.49	10.15
Hf	8.2	6.1	9.4	8.1	6.7	3.2	3.0	4.3	4.8	4.1	2.9
Ho	0.99	0.68	1.15	0.88	0.91	1.50	1.38	1.31	1.37	1.35	1.49
La	48.7	47.8	43.8	53.9	39.0	58.0	52.2	49.4	50.8	53.0	58.1
Lu	0.50	0.36	0.59	0.45	0.44	0.70	0.62	0.63	0.65	0.62	0.70
Nb	18.9	16.0	21.2	16.7	18.0	26.8	20.6	18.4	19.7	18.7	24.0
Nd	35.4	27.3	39.9	37.4	33.2	56.5	52.8	49.7	51.2	51.8	59.2
Pr	9.60	8.03	10.15	10.60	8.50	14.25	13.10	12.55	12.90	13.15	15.20
Rb	238	288	197.0	223	210	147.5	157.5	184.0	176.5	166.5	143.5
Sm	6.52	4.31	7.84	6.64	6.10	11.00	10.15	9.71	10.20	9.93	11.20
Sn	2	2	2	2	3	7	7	6	6	6	7
Sr	508	403	504	534	609	820	770	792	757	796	820
Ta	1.6	1.6	1.4	1.0	1.0	1.3	1.0	0.9	1.0	0.9	1.1
Tb	0.84	0.58	1.05	0.82	0.83	1.42	1.30	1.25	1.32	1.29	1.43
Th	12.75	25.6	10.35	16.70	12.85	7.61	6.83	8.11	8.18	6.92	7.72
Tm	0.45	0.32	0.54	0.44	0.42	0.68	0.62	0.56	0.61	0.59	0.67
U	2.73	4.63	2.53	2.92	2.53	2.68	2.25	2.23	2.14	1.68	2.17
V	38	25	44	32	51	132	146	151	136	142	140
W	2	2	2	2	7	2	3	3	5	3	2
Y	27.6	19.3	32.5	25.5	26.2	46.5	39.7	38.3	40.6	40.4	46.1
Yb	3.10	2.26	3.75	2.97	2.86	4.46	4.24	3.98	4.09	3.94	4.60
Zr	322	204	371	317	257	121	111	165	184	164	114

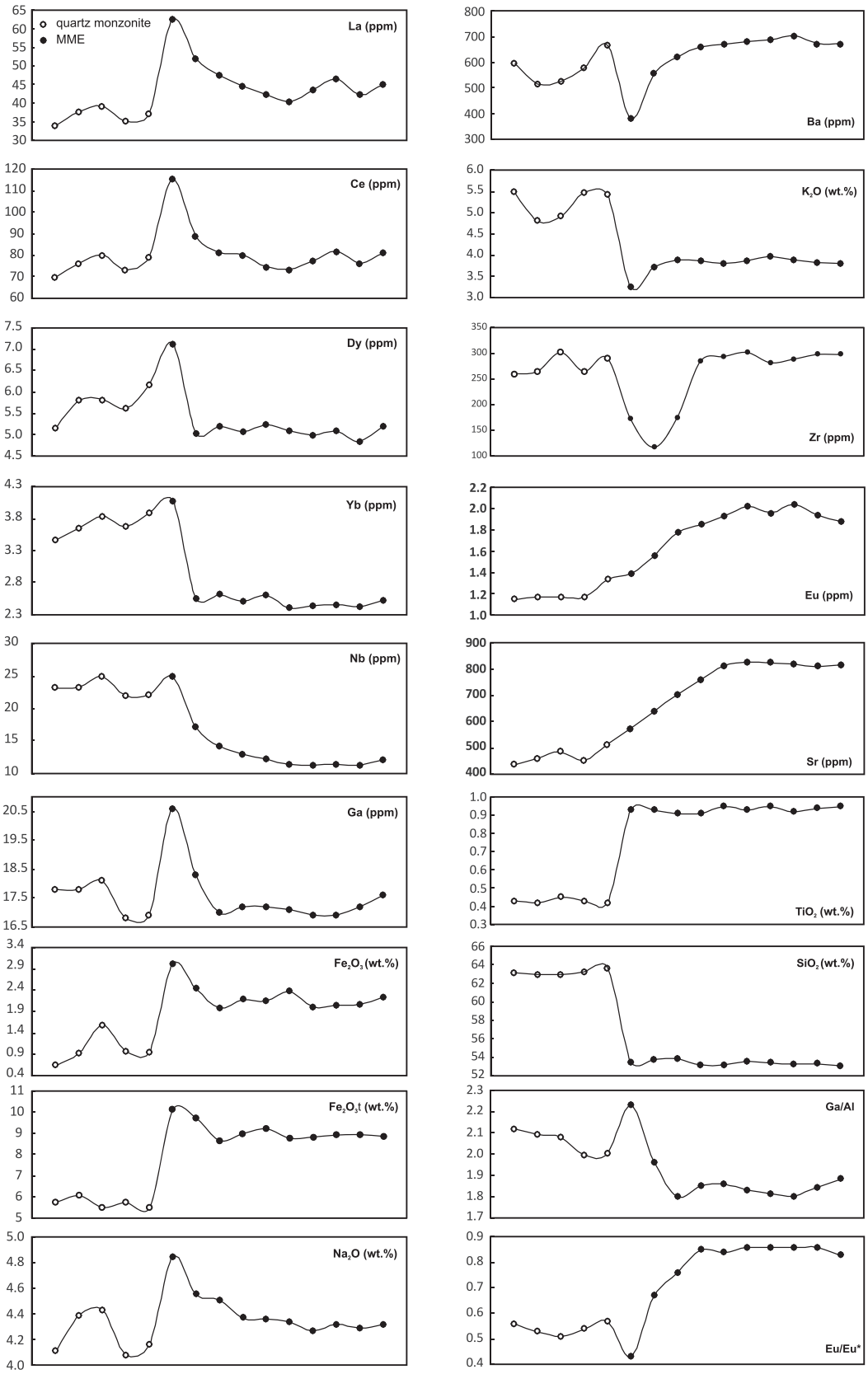

Fig. 8. Compositional profiles of the quartz monzonite-MME pair (17MC), showing four types. (1) uphill mass transfer profiles from the quartz monzonite to the MME, as exemplified by REE, Nb, Ga, Fe_2O_3 and Na_2O. (2) uphill mass transfer profiles from the MME to the quartz monzonite, as exemplified by Ba and K_2O. (3) monotonic profiles, as exemplified by Sr and Eu. (4) insignificant mass transfer profiles, as exemplified by TiO_2 and SiO_2. Note that the maximum/minimum concentrations of many elements occur at the contact, which cannot be explained by magma mixing. Compositional profiles of the quartz monzonite-MME pair (17HD, next page). Note that this late MME underwent stronger mass transfer with the host rock than the early one. The Ga/Al of MME has outweighed that of the host quartz monzonite and the MME has stronger negative Eu anomalies.

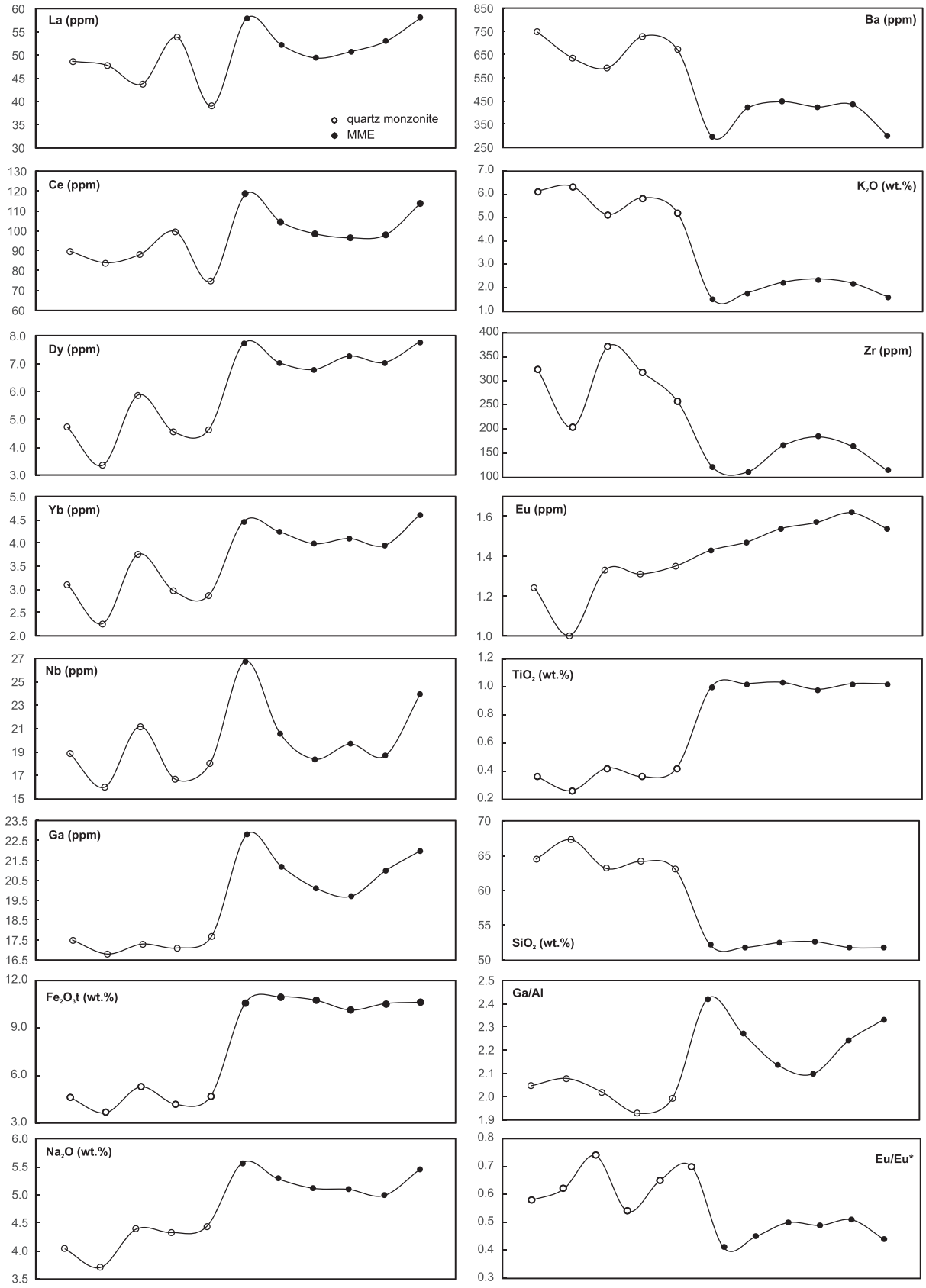

Fig. 8 (*continued*).

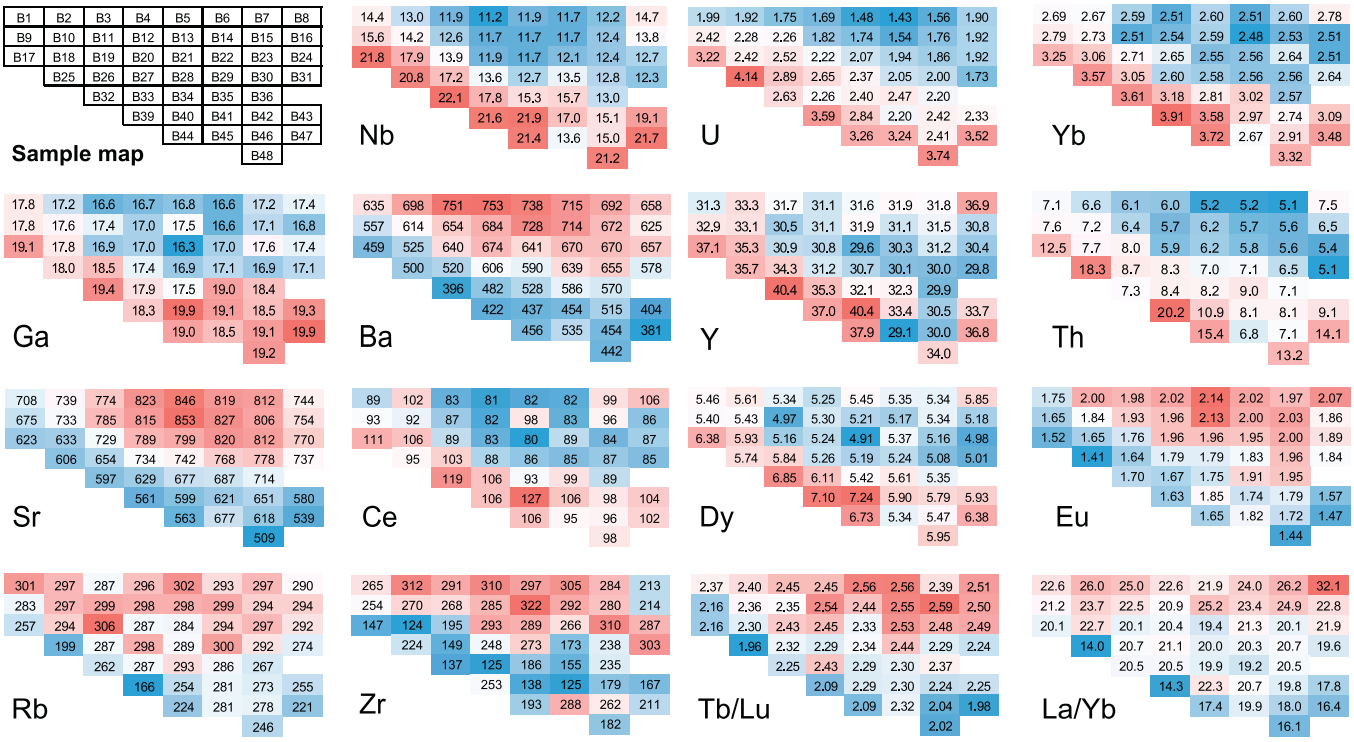

Fig. 9. Trace elemental mapping on a face of the MME (17MC), showing the compositional variations within the MME. Numbers represent trace elemental contents (ppm) or ratios. Red and blue colours represent high and low contents, respectively. Compare the sample map with Fig. 2C for the positions of the samples. Generally, the results are consistent with the one-dimensional profile in Fig. 8. At the margin of the MME, Nb, U, Th, REE (except for Eu), Y, Ga are higher; Ba, Sr, Eu, Rb and Zr are lower. Note that both MREE/HREE and LREE/HREE are lower at the margin of the MME, which can be explained by decreasing diffusion rates from La to Lu.

tends to reduce the difference between mafic and felsic magmas; however, uphill diffusion may occur during the magma mingling (Lesher, 1990), which is likely the case for MQM. Magma mixing and mingling, which are continuous and gradual during felsic-mafic magma interactions, may exert opposite influences on their geochemical evolutions. If the two processes work together during interaction between felsic and mafic magmas, curvilinear and scattered trends in the Harker diagrams are likely for the elements mobile during diffusion processes but the linear trends are still possible for immobile elements (Cramer and Kwak, 1988).

Baker (1990) argues the diffusions of major and trace elements are ineffective except for alkali metals. However, diffusion is considered as a principle mechanism to change the chemical composition of mingled magmas (Barbarin and Didier, 1992; Cramer and Kwak, 1988; Kumar and Rino, 2006; Tepper and Kuehner, 2004) and the "compositional integrity" is only restricted to some least mobile elements such as SiO_2 and TiO_2 (Cramer and Kwak, 1988). Crystallization fractionation or magma mixing produces linear major-trace element trends and different compositions for minerals in the enclaves and their hosts (Tindle, 1991). However, it is not the case for Muchen intrusion (Fig. 10). In contrast, diffusion is a necessary process for the magma differentiation of Muchen intrusion, which produces curvilinear major-trace element trends (Lesher, 1990) and compositional similarities of mafic silicates in enclaves and their hosts (Tindle, 1991). More sodic plagioclase at the rim of the MME (Fig. 6) can be explained by Ca diffusion towards the granitic melt and Na diffusion towards the mafic melt. The rim does not retain more primitive magma or mineral compositions. It therefore does not have obvious chilling features in spite of slightly finer-grained texture.

Some detailed petrographic and compositional features in the analyzed host-MME profiles further support diffusions play an important role in mass transfer during magma mingling. The different diffusion rates will cause that the compositional profiles of different elements are not coupled (Fig. 8), which is difficult to explain by reaction or metasomatic rim (Farner et al., 2014). It is notable that the high REE and HFSE concentrations in the MMEs (especially at the margins) may be explained by higher modal hornblende that is enriched in these elements (Davidson et al., 2007; Rollinson, 1993). However, as shown in the first MME-host pair, the compositional and modal profiles are not coupled (Figs. 4 and 8), where hornblende is restricted in a narrow range (within one cube sample). In addition, hornblende is more enriched in MREE (Davidson et al., 2007; Richards, 2011); however, the margin of the early-stage MME, where hornblende occurs, has lower MREE/HREE and LREE/HREE. Such a pattern cannot be an amphibole sequestering effect (Davidson et al., 2007) but most likely caused by a slight decrease of diffusivity from La to Lu (Zhang et al., 2010).

The compositions of hornblende in the MMEs and host granitoid imply an emplacement level of 3.1–3.6 km. A level of 6–7 km is estimated for the Muchen intrusion (Liu et al., 2013a) using the method of Johnson and Rutherford (1989), which may overestimate the pressure of hornblende crystallization (Ridolfi et al., 2009). These geobarometry results imply that extensive mass transfer between coeval felsic and mafic magmas may still occur at shallow crustal levels.

Petrographic and chemical differences between the MMEs in the two profiles are significant. In many cases the MME and host granitoid have the same mineral assemblage but in different proportions (Barbarin and Didier, 1992; Kumar and Rino, 2006; Vernon, 1984). This is the case only for one MME (17HD) in this study. For the other (17MC), occurrence of hornblende at the rim and clinopyroxene in the core reflect the equilibrium is not attained. The two MMEs represent late and early stage of magma mingling and interaction, which is further supported by the major and trace element patterns of the two MMEs. Inter-MME and intra-MME variations are large enough to demonstrate the role of magma mingling in changing the compositions of MMEs, as also shown by Cramer and Kwak (1988). For the MMEs, some major elements and most trace elements are significantly influenced by magma

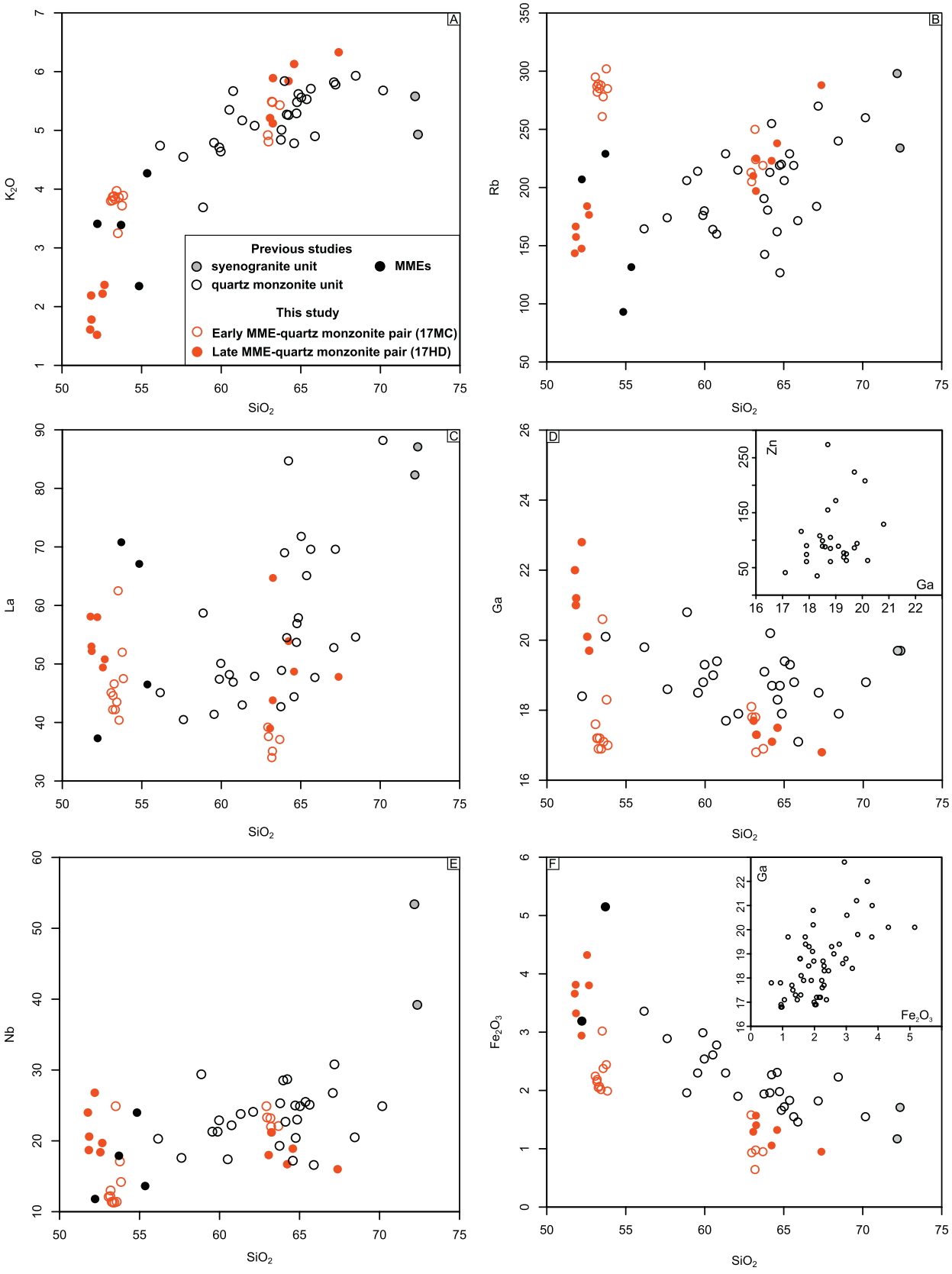

Fig. 10. Harker diagrams for the two MME-quartz monzonite pairs in the context of published intrusion-scale data (major elements in wt%, trace elements in ppm). A K_2O versus SiO_2. B Rb versus SiO_2. C La versus SiO_2. D Ga versus SiO_2, the inset showing Zn versus Ga. E Nb versus SiO_2. F Fe_2O_3 versus SiO_2, the inset showing Ga versus Fe_2O_3. The samples from the late-stage MME (17HD) have lower K_2O, Rb and higher La, Ga, Nb, Fe_2O_3 contents than the early-stage MME (17MC). Comparing with the quartz monzonite samples at the same SiO_2 contents, the ones as the host of MME swarms have high Rb and low La, Ga, Fe_2O_3 contents. The host of the late-stage MME (17HD) has high K_2O and low Nb contents. The differentiation of the samples most likely reflects the mass transfer between the mafic and felsic magmas. Ga is positively correlated with Zn and Fe_2O_3 for the Muchen intrusion.

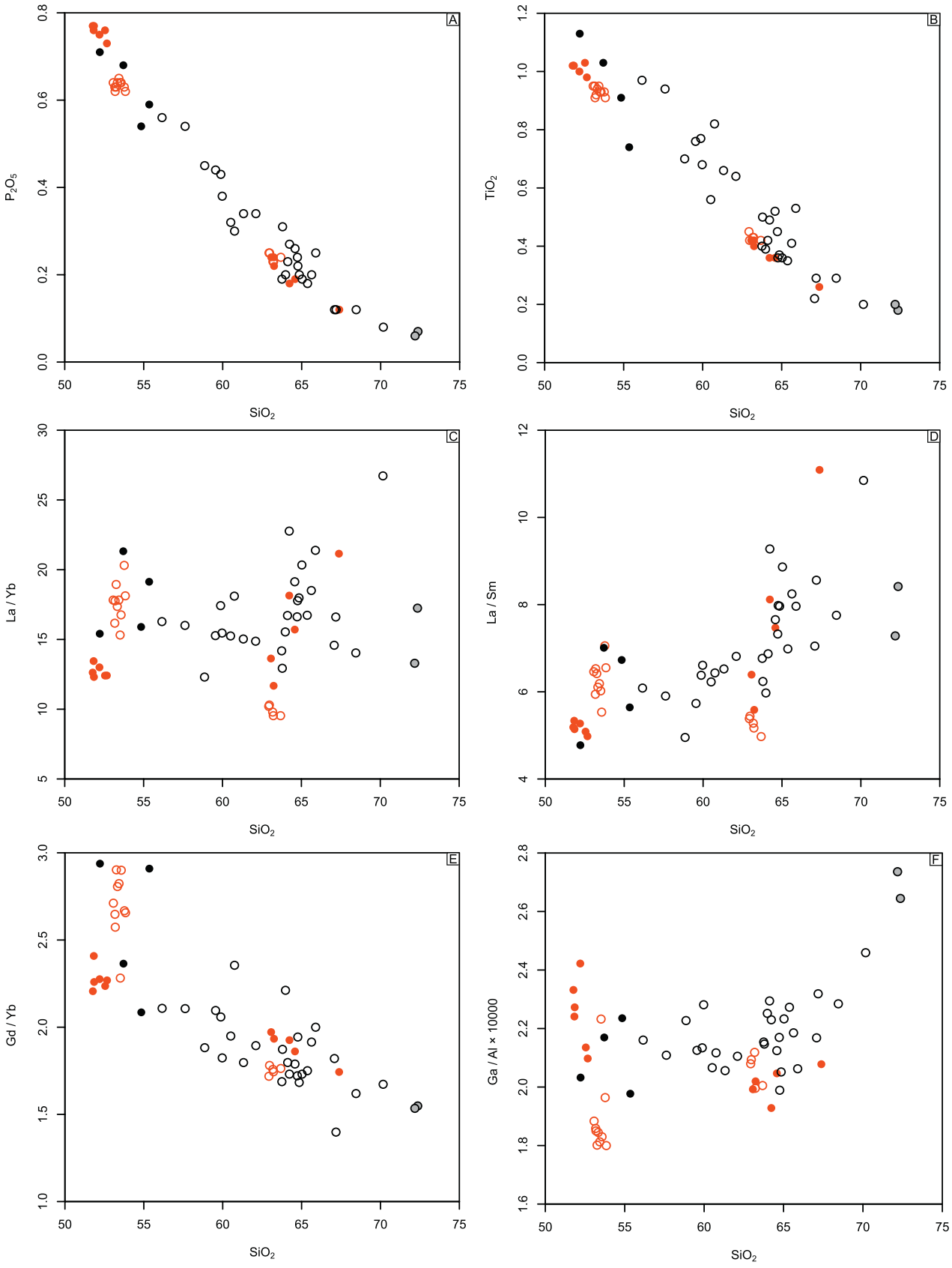

Fig. 11. Variations of some elemental concentrations and ratios with SiO_2 for the samples in Fig. 10 (using the same symbols, major elements in wt%, trace elements in ppm). A P_2O_5 versus SiO_2. B TiO_2 versus SiO_2. C La/Yb versus SiO_2. D La/Sm versus SiO_2. E Gd/Yb versus SiO_2. F Ga/Al × 10,000 versus SiO_2. Relative to the samples from the early-stage MME (17MC), the late-stage ones (17HD) have lower La/Yb, La/Sm, Gd/Yb and higher Ga/Al. The samples with the minimum P_2O_5, TiO_2, La/Yb, La/Sm and Ga/Al are from the quartz monzonite that are the host of the MMEs. However, these samples have comparable Gd/Yb to those without MMEs.

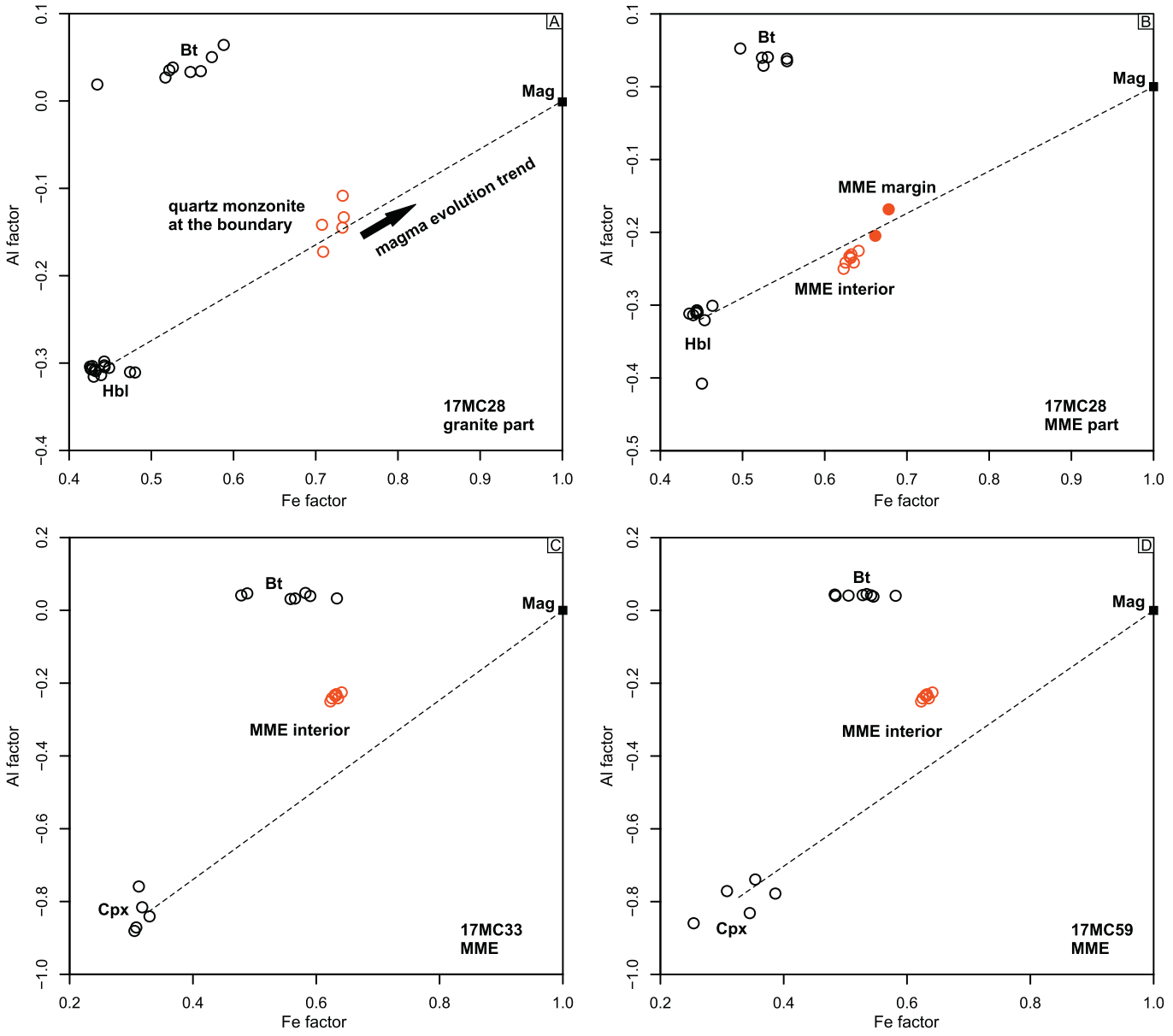

Fig. 12. Modified AFM diagrams (Cramer and Kwak, 1988) for the MME-quartz monzonite pair (17MC), showing the whole-rock and mineral compositions. Al-factor = molar (Al_2O_3 – CaO – Na_2O – K_2O) / (FeO_t + MgO), Fe-factor = molar FeO_t / (FeO_t + MgO), assuming magnetite as Fe_3O_4. A the compositions of bulk rock and mafic silicates of the granite at the contact. The rarity of biotite in the sample is consistent with such a graphic analysis. With the quartz monzonite becoming more felsic, the bulk compositions evolve towards magnetite and cause higher proportions of magnetite in the ferromagnesian minerals. B the compositions of bulk rock and mafic silicates of the MME at the contact. Note that iron enrichment at the MME margin causes the mineral assemblage moving to magnetite, which explains higher magnetite contents at the margin of many MMEs in the Muchen intrusion. C and D the compositions of bulk rock and mafic silicates of the MME in the interior. In these samples, clinopyroxene is stable instead of hornblende and biotite has a higher mode.

mingling processes (Figs. 8, 9 and 10). The compositions of the MMEs change from alkali series to sub-alkali series and K_2O/Na_2O strongly decreases. The changes of La, Zr, Nb and Y contents will cause that many discrimination diagrams such as Meschede (1986) cannot be applied to these mafic rocks. Unlike other REE, Eu follows Sr in the processes, implying it is largely divalent. It causes negative Eu anomalies of the MME samples, which is even stronger than the host quartz monzonite (Fig. 8). The higher magnetite contents at the MME margin are also mentioned in Zhu et al. (2017b), which suggests it is an oxidized margin. However, the compositional profile of ferric iron implies that diffusion of ferric iron towards the MMEs is another factor for high magnetite contents at their margins (Fig. 8). It is argued that the higher oxidation states of arc lavas are partly caused by shallow-level differentiation processes (Lee et al., 2010). Ferric iron diffusion, from oxidized crustal melts to reduced mantle melts, provides an oxidization mechanism for basalt, which may be partly responsible for low Fe/Mg of the arc-related granitoids (Frost et al., 2001; Frost and Frost, 2008, 2011).

How the magma mingling may change the host granitoid is reported by few studies (Didier and Barbarin, 1991). Intrusion-scale whole-rock data is not discussed in Cramer and Kwak (1988). The elements such as Ga, Rb, La, Nb have higher or lower contents for the quartz monzonite samples close to the MMEs (Fig. 10). Although it appears that P_2O_5 and TiO_2 appear inert in the mass transfer processes between MME and the host rocks (Fig. 8, also see Cramer and Kwak, 1988). Their contents are also similar for the early and late MMEs (Fig. 11A and B). However, from the intrusion scale, the granitic samples close to the MMEs do have lower P_2O_5 and TiO_2 contents, implying their migration from the felsic to mafic magmas had already occurred at deeper levels and perhaps higher temperatures. Such uphill transfer of P_2O_5 and TiO_2 has been noticed by Key (1977) and this promotes crystallization of abundant apatite occurring in the MMEs.

The results demonstrate the magma mingling likely causes differentiation of the host granitic magmas at least at a decimeter scale. Such a scale is no long trivial comparing to what is shown by Baker (1990). The characteristic distance for diffusion is proportional to $(Dt)^{0.5}$ (Philpotts and Ague, 2009), where diffusion coefficient (D) and time (t) are expected to be large in a plutonic system of an active continental margin. High water contents in these subduction-related magmas and convective magma movement may significantly increase the effect of diffusion and mass transfer rates (Watson, 1981). Linear geochemical data should be expected during magma mixing (Langmuir et al., 1978; Wilcox, 1979) and scattered data are used to rule out magma mixing (Clemens et al., 2016b). However, mass transfer during magma mingling, which often accompanies magma mixing, may explain the complex and non-linear data sets.

5.2. Syenogranite of the Muchen intrusion: A unit escaping significant diffusion differentiation?

Besides the quartz monzonite as the major part of the Muchen intrusion, several syenogranite stocks intruded the quartz monzonite (Fig. 1B). The zircon U—Pb ages, zircon Hf isotopes, whole-rock Sr-Nd-Pb isotopes, hornblende compositions (Fig. 7B) are similar for the two units (Zhu et al., 2017b). It implies that they are in (partial) equilibrium in terms of isotopes and intensive parameters. Remelting of Muchen quartz monzonite to generate the syenogranite is not a feasible explanation, since such a mechanism should not cause similar intensive parameters for two magmas. In many aspects, the samples from the syenogranite unit show aluminous A-type features (King et al., 1997; Whalen et al., 1987), including high SiO_2, low Ca, low Sr, high REE with a strong negative Eu anomaly, high Nb and high Ga (and Ga/Al). In addition, the syenogranite samples show leaps in Harker diagrams relative to the quartz monzonite samples, which do not imply crystallization fractionation. From a geochemical perspective, the syenogranite may represent an independent hot-dry-reduced magma (Bachmann and Bergantz, 2008). However, occurrence of hornblende with similar compositions to those in the quartz monzonite (a wet and oxidized I-type), high modal magnetite and low zircon saturation temperatures contradict such a model. Since aforementioned diffusion processes will shift most characteristics of A-type to those of I-type, it is likely the absence of extensive diffusion between felsic-mafic magmas that retained the "A-type" features of the syenogranite, although relative short interaction time has achieved equilibrium for isotopes, temperatures, water and oxygen fugacities. Therefore, "A-type granite" such as the unit in the Muchen intrusion, does not necessarily imply a special crustal melting condition or a special tectonic setting. In contrast, the quartz monzonite unit, to different degrees, underwent the magma mixing-mingling processes and developed distinctly low REE, Nb, Ga/Al and high K. The MME or MME swarms currently hosted in the quartz monzonite simply fingerprinted such processes at shallow levels; more extensive felsic-mafic magma interactions likely occurred at deeper levels.

5.3. Impacts of magma mingling on some key ratios of granitoids

The concentrations and ratios of REE are often used to infer magma and tectonic processes. For instance, low Y, Yb and high La/Yb feature adakite or adakitic rocks (Castillo, 2006). The ratios such as La/Yb and Dy/Yb are used to discuss the roles of garnet and amphibole in magma and crustal thickening/attenuation processes (Davidson et al., 2007; Gill, 1981; He et al., 2011; Larocque and Canil, 2010; Mamani et al., 2010). A high La/Sm is linked to source enrichment (Kay et al., 2010). High and low REE contents in felsic rocks are linked to amphibole/titanite crystallization fractionation (Bachmann and Bergantz, 2008; Glazner et al., 2008; Richards, 2011). High Ga/Al is the diagnostic feature of A-type granitoids whereas I-type granitoids feature low Ga/Al (Whalen et al., 1987). A tendency has been often noted that Ga and Ga/Al increase during magma fractionation (Cocco et al., 1972); however, such a trend is undetectable or reverse in some instances. For many I-type granitoids, magma mingling and mass transfer likely occurred in both shallow levels and deep hot zones (Annen et al., 2006); however, their roles in changing REE patterns and Ga/Al are rarely discussed.

As shown in Fig. 11F, the quartz monzonite samples adjacent to the MMEs have lower La/Yb, La/Sm and Ga/Al. For MQM, diffusion during magma mingling, rather than garnet fractionation or source variation, is more likely responsible for the granitoid differentiation in terms of these ratios. On one hand, such a mechanism depresses A-type, source enrichment as well as garnet signals; on the other hand, MREE/HREE of the granitoids is not significantly influenced and may still constrain the existence of garnet during magma fractionation processes (Mamani et al., 2010; Zhu et al., 2014, 2016). Preferential partition of REE in the MMEs, and perhaps more importantly, in the basaltic magmas underplating the crustal hot zones, may be another important factor controlling the REE budget in continental arc magma system. Comparing with Early Cretaceous MME-rich granitoids in eastern South China, such as the MQM in this study, the Late Triassic orogenic MME-absent granitoids in the same region feature high MREE/HREE and high HREE contents (Zhu et al., 2017b). It is therefore questionable whether garnet is solo responsible for low HREE content and strong REE fractionation.

Ga and Al, through magma mingling processes, are greatly differentiated. It caused low ratios in the granitoids and high ratios in the mingled mafic rocks for the MQM, which may be also true in many other cases (Kumar and Rino, 2006; Moita et al., 2015; Zhang et al., 2005). In South China, MMEs are much more common in I-type granitoids than A-type granitoids (mostly aluminous A-type). Rarity of magma mingling in A-type granitoids and low diffusion rates in these water-poor magmas will cause a high Ga/Al. High Ga/Al of the Late Triassic orogenic MME-absent granitoids in eastern South China (Zhu et al., 2016) may be caused by such a mechanism, although they are regarded by some studies as anorogenic A-type granites (Li et al., 2012; Sun et al., 2011). For the Muchen intrusion, Zn and Fe_2O_3 are both positively corelated with Ga (Fig. 10D, F), implying their concentrations may be also influenced by diffusion processes. Relative high Zn and Fe_2O_3 contents in A-type granitoids (Table 1 in Whalen et al., 1987) may suggest absence or inefficiency of diffusions between felsic and mafic magmas.

Zr, Ti and their ratio may significantly change, especially for MMEs, in magma mingling processes (Fig. 8). Unlike other HSFE, Zr and Hf transferred from the MMEs to the host quartz monzonite. This is similar to the situation of Tepper and Kuehner (2004), most likely reflecting sequestering of Zr and Hf in early-formed zircon in the host rocks. However, initial Zr enrichment, such as high Zr content partially kept in the core of early MMEs, may be caused by reverse transfer at high temperature (crustal melting during basaltic underplating?). It is uncertain to use these "mobile" elements in the rock classification and tectonic discrimination (Meschede, 1986; Winchester and Floyd, 1977).

Another notable point from the compositional profiles and mapping of this study is that Lu is strongly fractionated from Hf in the MMEs. It is likely caused by low chemical potential of Hf in the granitic melt due to zircon crystallization (Tepper and Kuehner, 2004). For the early MME, Lu/Hf ranges from 0.06 at the core to 0.14 at the rim; for the late MME, Lu/Hf ranges from 0.14 at the core to 0.24 at the rim. As a result, $^{176}Lu/^{177}Hf$ ($= 0.142 \times Lu/Hf$) ranges from 0.008 to 0.034 for different parts of two sampled MMEs and actual range should be wider. Such a large range of $^{176}Lu/^{177}Hf$ will cause a strong Hf isotopic variation in the future melting events. In contrast, Sm and Nd do not fractionate in such processes, which may cause decoupled Nd—Hf isotopic features.

6. Conclusions

The coeval nature of MME and host quartz monzonite is supported by the same zircon U—Pb age, the rounded to ellipsoidal shape of

MME without solid-state deformation texture and similar magnetic fabrics. Despite quench textures such as fine grains and acicular apatite, the mafic and felsic magmas achieved partial equilibrium in terms of isotopes and intensive parameters (temperature, pressure, oxygen and water fugacities). During the equilibrium processes, elemental diffusion caused enrichment of REE, Y, Nb, Ta, Ga, Na_2O, Fe^{3+} and depletion of K_2O, Sr, Ba, Rb in the MMEs. The compositions of the MMEs change from alkali to sub-alkali and K_2O/Na_2O significantly decreases. For the quartz monzonite host of the MMEs, K_2O and Rb contents increased; LREE, Nb and Ga decreased. These trends are more significant comparing with the syenogranite unit of the Muchen intrusion, which likely escaped extensive diffusions with coeval mafic magmas. The elemental differentiation during magma mingling probably explains non-linear trends in Harker diagrams for the magma mixing system. In addition, elemental differentiation during magma mingling influenced many key elemental contents or ratios with petrogenetic or tectonic significance, such as REE, Nb, Zn, La/Yb, Lu/Hf, Eu/Eu*, Ga/Al and Fe^{3+}/Fe^{2+}. Higher Ga and Ga/Al in the mafic members of some magmatic series may be caused by diffusional enrichment, which also explains rarity of high Ga/Al (A-type) granitoids in arc environments. Such a mechanism should be also common and even more extensive in the deep hot zones of the continental crust with basaltic underplating.

Acknowledgements

This work was financially supported by the National Natural Science Foundation of China (41602050), the Zhejiang Provincial Natural Science Foundation of China (LY15D020002) and the Fundamental Research Funds for the Central Universities (2015QNA3018). The comments from Nelson Eby and two anonymous reviewers greatly improve the manuscript.

Appendix A. Supplementary data

Supplementary data to this article can be found online at https://doi.org/10.1016/j.lithos.2018.07.033.

References

Abdel-Rahman, A.-F.M., 1994. Nature of biotites from alkaline, calc-alkaline, and peraluminous magmas. J. Petrol. 35, 525–541.
Anderson, J.L., Barth, A.P., Wooden, J.L., Mazdab, F., 2008. Thermometers and thermobarometers in granitic systems. Rev. Mineral. Geochem. 121–142.
Annen, C., Blundy, J.D., Sparks, R.S.J., 2006. The genesis of intermediate and silicic magmas in deep crustal hot zones. J. Petrol. 47, 505–539.
Ayrton, S.N., 1991. Appinites, lamprophyres and mafic microgranular enclaves: three related products of interaction between acid and basic magmas. In: Didier, J., Barbarin, B. (Eds.), Enclaves and Granite Petrology. Elsevier, Amsterdam, pp. 465–476.
Bachmann, O., Bergantz, G.W., 2008. Rhyolites and their source mushes across tectonic settings. J. Petrol. 49, 2277–2285.
Baker, D.R., 1990. Chemical interdiffusion of dacite and rhyolite: anhydrous measurements at 1 atm and 10 kbar, application of transition state theory, and diffusion in zoned magma chambers. Contrib. Mineral. Petrol. 104, 407–423.
Barbarin, B., Didier, J., 1992. Genesis and evolution of mafic microgranular enclaves through various types of interaction between coexisting felsic and mafic magmas. Earth Environ. Sci. Transact. Roy. Soc. Edinburgh 83, 145–153.
Castillo, P., 2006. An overview of adakite petrogenesis. Chin. Sci. Bull. 51, 257–268.
Chappell, B.W., White, A.J.R., Wyborn, D., 1987. The importance of residual source material (restite) in granite petrogenesis. J. Petrol. 28, 1111–1138.
Clemens, J.D., Maas, R., Waight, T.E., Kunneke, L.K., 2016a. Genesis of felsic plutonic magmas and their igneous enclaves: the Cobaw batholith of southeastern Australia. J. Geol. 124, 293–311.
Clemens, J.D., Regmi, K., Nicholls, I.A., Weinberg, R., Maas, R., 2016b. The Tynong pluton, its mafic synplutonic sheets and igneous microgranular enclaves: the nature of the mantle connection in I-type granitic magmas. Contrib. Mineral. Petrol. 171, 35.
Clemens, J.D., Stevens, G., Elburg, M.A., 2017. Petrogenetic processes in granitic magmas and their igneous microgranular enclaves from Central Victoria, Australia: match or mismatch? Trans. Roy. Soc. South Africa 72, 6–32.
Cocco, G., Fanfani, L., Zanazzi, P.F., 1972. Elements Cr (24) to Br (35). Handbook of Geochemistry. vol. 2. Springer-Verlag (897 pp).
Cox, K.G., Bell, J.D., Pankhurst, R.J., 1979. The Interpretation of Igneous Rocks. Allen and Unwin, London (450 pp).
Cramer, J.J., Kwak, T.A.P., 1988. A geochemical study of zoned inclusions in granitic rocks. Am. J. Sci. 288, 827–871.
Davidson, J., Turner, S., Handley, H., Macpherson, C., Dosseto, A., 2007. Amphibole "sponge" in arc crust? Geology 35, 787–790.
Deer, W.A., Howie, R.A., Zussman, J., 1962. Rock-Forming Minerals: Sheet Silicates. Longmans (270 pp).
Didier, J., Barbarin, B., 1991. Enclaves and Granite Petrology. Elsevier (625 pp).
Don, S., Crambes, C., Tait, S., Wiebe, R.A., 1997. Magma mingling in dikes and sills. J. Geol. 105, 75–86.
Farner, M.J., Lee, C.-T.A., Putirka, K.D., 2014. Mafic–felsic magma mixing limited by reactive processes: a case study of biotite-rich rinds on mafic enclaves. Earth Planet. Sci. Lett. 393, 49–59.
Frost, B.R., Frost, C.D., 2008. A geochemical classification for feldspathic igneous rocks. J. Petrol. 49, 1955–1969.
Frost, C.D., Frost, B.R., 2011. On ferroan (A-type) Granitoids: their compositional variability and modes of origin. J. Petrol. 52, 39–53.
Frost, B.R., Barnes, C.G., Collins, W.J., Arculus, R.J., Ellis, D.J., Frost, C.D., 2001. A geochemical classification for granitic rocks. J. Petrol. 42, 2033–2048.
Gao, W., Wang, Z., Wang, D., Li, C., 2014. Zircon U-Pb geochronology, geochemistry of late-Mesozoic granite in southeastern (SE) Zhejiang Province and its tectonic implication. J. Jilin Univ. 44, 861–875.
Gill, J.B., 1981. Orogenic Andesites and Plate Tectonics, 16. Springer Verlag (390 pp).
Glazner, A.F., Coleman, D.S., Bartley, J.M., 2008. The tenuous connection between high-silica rhyolites and granodiorite plutons. Geology 36, 183–186.
He, Y., Li, S., Hoefs, J., Huang, F., Liu, S.-A., Hou, Z., 2011. Post-collisional granitoids from the Dabie orogen: new evidence for partial melting of a thickened continental crust. Geochim. Cosmochim. Acta 75, 3815–3838.
Hibbard, M.J., 1991. Textural anatomy of twelve magma-mixed granitoid systems. In: Didier, J., Barbarin, B. (Eds.), Enclaves and Granite Petrology. Elsevier, Amsterdam, pp. 431–444.
Hsieh, P.-S., Chen, C.-H., Yen, C.-M., Lee, C.-Y., 2009. Origin of mafic microgranular enclaves (MMEs) and their host rocks of the cretaceous Xiaojiang-Liangnong granitic complexes in the southeast coast magmatic belt, S China. Terr. Atmos. Ocean. Sci. 20, 480–500.
Ishihara, S., Hashimoto, M., Machida, M., 2000. Magnetite/ilmenite–series classification and magnetic susceptibility of the Mesozoic-Cenozoic batholiths in Peru. Resour. Geol. 50, 123–129.
Jerram, D., Petford, N., 2011. The Field Description of Igneous Rocks. Wiley-Blackwell (238 pp).
Johnson, M.C., Rutherford, M.J., 1989. Experimental calibration of the aluminum-in-hornblende geobarometer with application to Long Valley caldera (California) volcanic rocks. Geology 17, 837–841.
Kay, S.M., Coira, B.L., Caffe, P.J., Chen, C.-H., 2010. Regional chemical diversity, crustal and mantle sources and evolution of central Andean Puna plateau ignimbrites. J. Volcanol. Geotherm. Res. 198, 81–111.
Key, C.H., 1977. Origin of appinitic pockets in the diorites of Jersey, Channel Islands. Mineral. Mag. 41, 183–192.
King, P.L., White, A.J.R., Chappell, B.W., Allen, C.M., 1997. Characterization and origin of aluminous A-type granites from the Lachlan Fold Belt, southeastern Australia. J. Petrol. 38, 371–391.
Kumar, S., Rino, V., 2006. Mineralogy and geochemistry of microgranular enclaves in Palaeoproterozoic Malanjkhand granitoids, central India: evidence of magma mixing, mingling, and chemical equilibration. Contrib. Mineral. Petrol. 152, 591–609.
Langmuir, C.H., Vocke, R.D., Hanson, G.N., Hart, S.R., 1978. A general mixing equation with applications to Icelandic basalts. Earth Planet. Sci. Lett. 37, 380–392.
Larocque, J., Canil, D., 2010. The role of amphibole in the evolution of arc magmas and crust: the case from the Jurassic Bonanza arc section, Vancouver Island, Canada. Contrib. Mineral. Petrol. 159, 475–492.
Lee, C.-T.A., Luffi, P., Le Roux, V., Dasgupta, R., Albarede, F., Leeman, W.P., 2010. The redox state of arc mantle using Zn/Fe systematics. Nature 468, 681–685.
Lesher, C.E., 1990. Decoupling of chemical and isotopic exchange during magma mixing. Nature 344, 235–237.
Li, Z.-X., Li, X.-H., 2007. Formation of the 1300-km-wide intracontinental orogen and postorogenic magmatic province in Mesozoic South China: a flat-slab subduction model. Geology 35, 179–182.
Li, X.-H., Li, W.-X., Li, Z.-X., Lo, C.-H., Wang, J., Ye, M.-F., Yang, Y.-H., 2009. Amalgamation between the Yangtze and Cathaysia blocks in South China: constraints from SHRIMP U-Pb zircon ages, geochemistry and Nd-Hf isotopes of the Shuangxiwu volcanic rocks. Precambrian Res. 174, 117–128.
Li, Z.-X., Li, X.-H., Wartho, J.-A., Clark, C., Li, W.-H., Zhang, C.-L., Bao, C.-M., 2010. Magmatic and metamorphic events during the early Paleozoic Wuyi-Yunkai orogeny, southeastern South China: new age constraints and pressure-temperature conditions. Geol. Soc. Am. Bull. 122, 772–793.
Li, W.-Y., Ma, C.-Q., Liu, Y.-Y., Robinson, P., 2012. Discovery of the Indosinian aluminum A-type granite in Zhejiang Province and its geological significance. Sci. China Earth Sci. 55, 13–25.
Liu, L., Qiu, J.-S., Li, Z., 2011. Zircon U-Pb age and Hf isotopic compositions of quartz monzonite and enclosed mafic enclaves in Muchen pluton, Zhejiang Province: tracing magma mixing in their petrogenesis. Geol. Rev. (in Chinese with English abstract) 57, 327–336.
Liu, L., Qiu, J.S., Li, Z., Li, Y.L., 2012. Petrogenesis of the early cretaceous quartz monzonite pluton at Muchen in Longyou County, Zhejiang Province: evidences from elemental and isotopic geochemistry of mafic microgranular enclaves and their host rocks. Acta Petrol. Sin. 28, 3993–4006.
Liu, L., Qiu, J.-S., Li, Z., 2013a. Origin of mafic microgranular enclaves (MMEs) and their host quartz monzonites from the Muchen pluton in Zhejiang Province, Southeast

China: implications for magma mixing and crust–mantle interaction. Lithos 160–161, 145–163.
Liu, L., Qiu, J.-S., Yang, Z.-L., 2013b. Petrogenesis of the Maoliling pluton in Linhai County, Zhejiang Province: constraints from geochronology, geochemistry and Sr-Nd-Hf isotopes. Acta Pet. Sin. 29, 4069–4086.
Lu, C.-Z., 2007. Geochemical characteristics and tectonic implications of Muchen quartz monzonite pluton in Zhejiang Province. Geochimica 36, 457–466.
Mamani, M., Wörner, G., Sempere, T., 2010. Geochemical variations in igneous rocks of the central Andean orocline (13°S to 18°S): tracing crustal thickening and magma generation through time and space. Geol. Soc. Am. Bull. 122, 162–182.
Meschede, M., 1986. A method of discriminating between different types of mid-ocean ridge basalts and continental tholeiites with the Nb-Zr-Y diagram. Chem. Geol. 56, 207–218.
Moita, P., Santos, J.F., Pereira, M.F., Costa, M.M., Corfu, F., 2015. The quartz-dioritic Hospitais intrusion (SW Iberian Massif) and its mafic microgranular enclaves — evidence for mineral clustering. Lithos 224-225, 78–100.
Peccerillo, A., Taylor, S., 1976. Geochemistry of Eocene calc-alkaline volcanic rocks from the Kastamonu area, northern Turkey. Contrib. Mineral. Petrol. 58, 63–81.
Philpotts, A.R., Ague, J.J., 2009. Principles of Igneous and Metamorphic Petrology. Cambridge University Press (667 pp).
Pin, C., 1991. Sr–Nd isotopic study of igneous and metasedimentary enclaves in some Hercynian granitoids from the Massif Central, France. In: Didier, J., Barbarin, B. (Eds.), Enclaves and Granite Petrology. Elsevier, Amsterdam, pp. 333–343.
Richards, J.P., 2011. High Sr/Y arc magmas and porphyry Cu ± Mo ± Au deposits: just add water. Econ. Geol. 106, 1075–1081.
Ridolfi, F., Renzulli, A., Puerini, M., 2009. Stability and chemical equilibrium of amphibole in calc-alkaline magmas: an overview, new thermobarometric formulations and application to subduction-related volcanoes. Contrib. Mineral. Petrol. 160, 45–66.
Rollinson, H., 1993. Using Geochemical Data: Evaluation, Presentation, Interpretation. Longman, London (352 pp).
Sun, Y., Ma, C.-Q., Liu, Y.-Y., She, Z.-B., 2011. Geochronological and geochemical constraints on the petrogenesis of late Triassic aluminous A-type granites in southeast China. J. Asian Earth Sci. 42, 1117–1131.
Tepper, Jeffrey H., Kuehner, Scott M., 2004. Geochemistry of mafic enclaves and host granitoids from the Chilliwack batholith, Washington: chemical exchange processes between coexisting mafic and felsic magmas and implications for the interpretation of enclave chemical traits. J. Geol. 112, 349–367.
Tindle, A.G., 1991. Trace element behaviour in microgranular enclaves from granitic rocks. In: Didier, J., Barbarin, B. (Eds.), Enclaves and Granite Petrology. Elsevier, Amsterdam, pp. 333–343.
Vernon, R.H., 1984. Microgranitoid enclaves in granites-globules of hybrid magma quenched in a plutonic environment. Nature 309, 438–439.
Watson, E.B., 1981. Diffusion in magmas at depth in the earth: the effects of pressure and dissolved H2O. Earth Planet. Sci. Lett. 52, 291–301.
Whalen, J.B., Currie, K.L., Chappell, B.W., 1987. A-type granites: geochemical characteristics, discrimination and petrogenesis. Contrib. Mineral. Petrol. 95, 407–419.
Wilcox, R.E., 1979. The liquid line of descent and variation diagrams. In: Yoder, H.S. (Ed.), Evolution of the Igneous Rocks (Fiftieth Anniversary Perspectives), pp. 205–232.
Winchester, J.A., Floyd, P.A., 1977. Geochemical discrimination of different magma series and their differentiation products using immobile elements. Chem. Geol. 20, 325–343.
Wones, D.R., 1981. Mafic silicates as indicators of intensive variables in granitic magmas. Min. Geol. 31, 191–212.
Wong, J., Sun, M., Xing, G.-F., Li, X.-H., Zhao, G.-C., Wong, K., Wu, F.-Y., 2011. Zircon U–Pb and Hf isotopic study of Mesozoic felsic rocks from eastern Zhejiang, South China: geochemical contrast between the Yangtze and Cathaysia blocks. Gondwana Res. 19, 244–259.
Yu, J.-H., O'Reilly, S.Y., Zhou, M.-F., Griffin, W.L., Wang, L., 2012. U–Pb geochronology and Hf–Nd isotopic geochemistry of the Badu Complex, southeastern China: implications for the Precambrian crustal evolution and paleogeography of the Cathaysia Block. Precambrian Res. 222–223, 424–449.
ZGS, 1966. Regional Geology of Jinhua Area, Zhejiang Province. Bureau of Geology and Mineral Resources of Zhejiang Province, Meicheng (117 pp).
Zhang, X.L., Qiu, J.S., Wang, D.Z., Wang, R.C., Xu, X.S., Chen, X.M., 2005. Geochemsitry and magmatic mixing of the Putuoshan biotite moyites and their enclaves, Zhejiang Province. Acta Petrol. Mineral. 24, 81–92.
Zhang, Y., Ni, H., Chen, Y., 2010. Diffusion data in silicate melts. Rev. Mineral. Geochem. 72, 311–408.
Zhou, X.-M., Li, W.-X., 2000. Origin of late Mesozoic igneous rocks in southeastern China: implications for lithosphere subduction and underplating of mafic magmas. Tectonophysics 326, 269–287.
Zhu, K.-Y., Li, Z.-X., Xu, X.-S., Wilde, S.A., 2014. A Mesozoic Andean-type orogenic cycle in southeastern China as recorded by granitoid evolution. Am. J. Sci. 314, 187–234.
Zhu, K.-Y., Li, Z.-X., Xu, X.-S., Wilde, S.A., Chen, H.-L., 2016. Early Mesozoic ferroan (A-type) and magnesian granitoids in eastern South China: tracing the influence of flat-slab subduction at the western Pacific margin. Lithos 240–243, 371–381.
Zhu, K.-Y., Li, M.-Y., Shentu, L.-F., Shen, Z.-Y., Yu, Y.-H., 2017a. Evaluation of a small-diameter sampling method in magnetic susceptibility, AMS and X-ray CT studies and its applications to mafic microgranular enclaves (MMEs) in granite. J. Volcanol. Geotherm. Res. 341, 208–227.
Zhu, K.-Y., Li, Z.-X., Xia, Q.-K., Xu, X.-S., Wilde, S.A., Chen, H.-L., 2017b. Revisiting Mesozoic felsic intrusions in eastern South China: spatial and temporal variations and tectonic significance. Lithos 294-295, 147–163.